Journal of the Brazilian Society of Mechanical Sciences and Engineering (2020) 42:519
https://doi.org/10.1007/s40430-020-02599-6

TECHNICAL PAPER

Effect of graphene nanoplatelet reinforcements on the dynamics of rotating truncated conical shells

Hassan Afshari[1]

Received: 17 March 2020 / Accepted: 1 September 2020 / Published online: 15 September 2020

Abstract

In this paper, a parametric study is presented for free vibration analysis of rotating truncated conical shells reinforced with graphene nanoplatelets (GNPs). The composite shell is considered to be composed of epoxy as the matrix and the GNPs which are distributed along the thickness direction based on the various distribution patterns. The shell is modeled based on the first-order shear deformation theory (FSDT), and effective material properties are calculated based on the Halpin–Tsai model and the rule of mixture. Incorporating centrifugal and Coriolis accelerations along with initial hoop tension, the set of the governing equations and boundary conditions are derived using Hamilton's principle and are solved numerically using generalized differential quadrature method. Convergence and accuracy of the presented solution are confirmed, and influences of various parameters on the forward and backward frequencies are investigated including circumferential mode number, boundary conditions, rotational speed, semi-vertex angle and also mass fraction, distribution pattern, width and thickness of the GNPs. It is noteworthy that for the first time, the initial hoop tension is incorporated for a rotating conical shell modeled based on the FSDT.

Keywords Vibration · Rotating conical shell · Coriolis acceleration · Initial hoop tension · Graphene nanoplatelets

1 Introduction

Due to their excellent mechanical and thermal properties, GNPs have been widely used as reinforcement in various engineering fields such as aerospace, automotive and civil engineering. Besides the experimental works on the material properties of GNP-reinforced composites, some theoretical and numerical works are presented on the mechanical behavior of such structures. Habibi et al. [1] studied wave propagation analysis of GNP-reinforced composite cylindrical nanoshells coupled with piezoelectric actuator and surrounded with viscoelastic foundation. They concluded that by adding GNPs in the pure epoxy matrix, the phase velocity of the nanoshells improves. Barati and Shahverdi [2] used finite element method (FEM) and studied forced vibration analysis of GNP-reinforced nanocomposite beams in thermal environments. They showed that dynamical deflection can be affected by weight fraction and distribution of GNPs, and resonance of nanocomposite beams can be controlled by the GNP content and distribution. Dynamic stability analysis of functionally graded (FG) porous arches reinforced with GNPs under the combined action of a static force and a dynamic uniform pressure in the radial direction was investigated by Zhao et al. [3]. They confirmed that stability of the porous arch can be enhanced by using symmetrically non-uniform porosity distribution and the addition of a small amount of GNPs. Afshari and Adab [4] presented exact solutions for size-dependent buckling and vibration analyses of GNP-reinforced rectangular microplates. It was shown by them that in order to have a better reinforcing effect, GNPs with larger surface area and fewer monolayer graphene sheets should be used. Static bending and free vibration analyses of FG porous plates reinforced with GNPs were studied by Nguyen et al. [5]. They confirmed that by adding a small amount of GNPs, the strength of FG plate structures can be significantly improved and distribution pattern of GNPs in matrix plays an important role in reinforcement. Shokrgozar et al. [6] studied viscoelastic

Technical Editor: Thiago Ritto.

✉ Hassan Afshari
hassan.afshari@iaukhsh.ac.ir

[1] Department of Mechanical Engineering, Khomeinishahr Branch, Islamic Azad University, Khomeinishahr/Isfahan, Iran

dynamics and static responses of GNP-reinforced composite cylindrical microshells. They concluded that viscoelastic foundation, distribution pattern of GNPs, boundary condition and weight function of GNPs have remarkable effects on the stability of the GNP-reinforced cylindrical microshells. Tabatabaei Nejhad et al. [7] studied out-of-plane vibration analysis of laminated GNP-reinforced composite curved beams bonded by piezoelectric layers. It was revealed by them that by using only one percent weigh fraction of GNPs, natural frequencies increase about 100% regardless of GNPs distribution pattern.

Dynamic analysis of rotating shells is one the most practical and interesting problems in mechanical engineering, and there are a considerable number of paper regarding vibration analysis of rotating shells. Rotating shells have been extensively used in mechanical and aerospace applications, such as high-speed centrifugal separator, advanced gas turbine and high-power aircraft jet engine. The dynamics of rotating cylindrical shells have received much attention over the recent years. Hosseini-Hashemi [8] presented an exact analytical solution for free vibration analysis of rotating FG cylindrical shells. They concluded that unlike the transverse modes, rotational speed has no effect on the axial modes. Free vibration analysis of rotating FG GNP-reinforced porous cylindrical shells was studied by Dong et al. [9]. They discussed on the effect of initial hoop tension on the natural frequencies of the rotating cylindrical shells and concluded that initial hoop tension makes the critical rotating speed vanishes in some modes. Dong et al. [10] presented an analytical solution on linear and nonlinear free vibration analysis and dynamic responses of rotating FG GNP-reinforced cylindrical shells with various boundary conditions and subjected to a static axial load. They showed that subjoining a small amount of GNPs increases both linear and nonlinear frequencies and reduces the nonlinear to linear frequency ratio. Qin et al. [11] studied wave propagation in rotating FG GNP-reinforced composite cylindrical shells with general boundary conditions and confirmed that the natural frequencies increase by increasing boundary spring stiffness and weigh fraction of GNPs. An analytical study was presented by Dong et al. [12] to predict the low-velocity impact response of rotating FG GNP-reinforced cylindrical shells subjected to impact, external axial and thermal loads. It was shown by them that the peak values of the radial displacement of load points and the contact duration decrease with increase in weight fraction of GNPs. In comparison with the rotating cylindrical shells, there are fewer number of works regarding dynamics of rotating conical shells. Qinkai and Fulei [13] studied dynamic stability analysis of rotating truncated conical shells subjected to a periodic axial load and presented a parametric study on the effects of rotational speed, constant axial load and geometrical parameters on the location and width of instability regions. They showed that increase in rotational speed of the shell leads to movements of instability region along the frequency axis, while it has no considerable effect on the width of instability region. Malekzadeh and Heydarpour [14] studied free vibration analysis of rotating FG-truncated conical shells with different boundary conditions. They concluded that with increase in rotational speed of the shell, the effect of Coriolis acceleration on the natural frequencies increases and its impact depends on the shell boundary conditions. Heydarpour et al. [15] studied free vibration analysis of rotating truncated conical shells reinforced with carbon nanotubes (CNTs) and focused on the influences of angular velocity, Coriolis acceleration, geometrical parameters, distribution pattern and volume fraction of CNTs on the natural frequencies of the shell. They showed that effects of volume fraction and distribution of CNTs depend on the semi-vertex angle and angular velocity of the shell. With assumption of temperature-dependent material properties, Shakouri [16] studied free vibration analysis of FG rotating conical shells in thermal environment and concluded that reduction in natural frequencies created by temperature rise would be attenuated as the rotational speed of the shell increases.

Reduction in weight and increase in strength and stiffness of structures is one of the most important challenges for mechanical engineers which has been solved in the recent years using multi-phase materials [17–19] and different types of nano-reinforcements such as single-walled carbon nanotubes (SWCNTs), multi-walled carbon nanotubes (MWCNTs) and GNPs. In comparison with SWCNTs and MWCNTs, GNPs have bigger specific surface area which creates stronger bonding with the matrix and significantly enhanced load transfer capability [20]. Thus, a truncated conical shell made of a low-density polymer enriched with GNPs can be considered as a good choice to increase the strength and stiffness and decrease the weight of rotating shells. It can be seen in the literature review that free vibration analysis of rotating GNP-reinforced truncated conical shells is not studied which is the topic of the presented paper. The shell is modeled based on the FSDT, and effective mechanical properties are estimated based on the Halpin–Tsai model along with the rule of mixture. The set of the governing equations are solved analytically in circumferential direction via appropriate harmonic functions and are solved numerically in meridional direction via GDQM. Effects of various geometrical parameters of the shell and distribution pattern, mass fraction and dimensional parameters of the GNPs on the forward and backward frequencies are investigated. In most of the papers regarding vibration analysis of rotating shells, the initial hoop tension is modeled based on the classical shells theories, and recently, some authors have modeled the initial hoop tension in rotating cylindrical shells based on the FSDT [9–12]. To the best knowledge of author, this paper is the first attempt to model the initial hoop tension in a rotating conical shell modeled based on the FSDT.

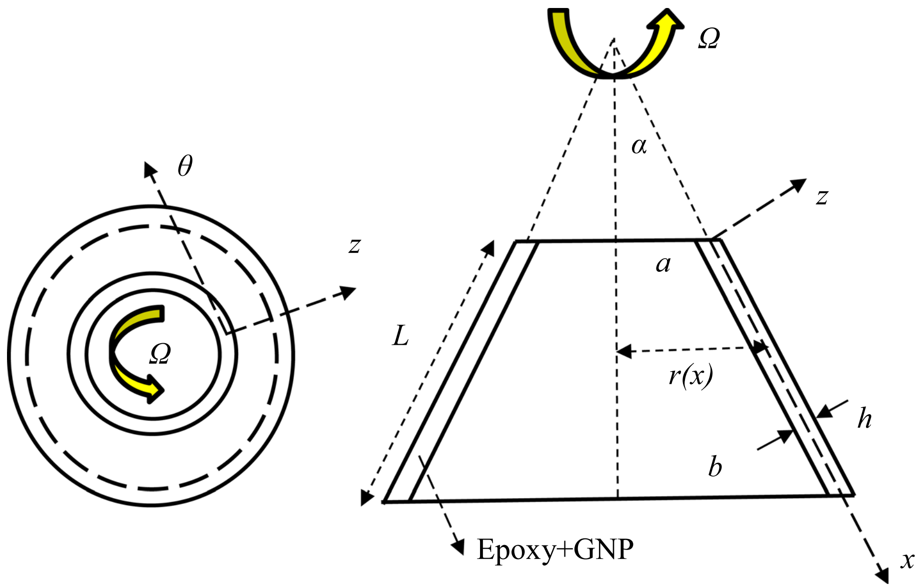

Fig. 1 Rotating GNP-reinforced truncated conical shell

Components of the strain can be stated as [22]

$$\begin{aligned}&\varepsilon_{xx}=\frac{\partial u}{\partial x}+\left(z-z_0\right)\frac{\partial\phi_x}{\partial x},\ \varepsilon_{\theta\theta}=\frac{\sin\alpha}{r}u+\frac{1}{r}\frac{\partial v}{\partial\theta}+\frac{\cos\alpha}{r}w+\left(z-z_0\right)\left(\frac{\sin\alpha}{r}\phi_x+\frac{1}{r}\frac{\partial\phi_\theta}{\partial\theta}\right),\\&\gamma_{x\theta}=\frac{1}{r}\frac{\partial u}{\partial\theta}+\frac{\partial v}{\partial x}-\frac{\sin\alpha}{r}v+\left(z-z_0\right)\left(\frac{1}{r}\frac{\partial\phi_x}{\partial\theta}+\frac{\partial\phi_\theta}{\partial x}-\frac{\sin\alpha}{r}\phi_\theta\right),\\&\gamma_{xz}=\frac{\partial w}{\partial x}+\phi_x,\ \gamma_{\theta z}=-\frac{\cos\alpha}{r}v+\frac{1}{r}\frac{\partial w}{\partial\theta}+\phi_\theta;\end{aligned}\tag{3}$$

2 Governing equations

As depicted in Fig. 1, a truncated conical shell of small radius a, large radius b, semi-vertex angle α, length L and thickness h rotating at constant angular velocity Ω is considered. The radius of the shell changes linearly as $r(x)=a+x sin\alpha$, and the shell is considered to be made of epoxy enriched with GNPs.

Based on the FSDT and incorporating effect of the neutral surface ($z=z_0$), displacement filed in the shell can be considered as

$$\begin{aligned}&u_1(x,\theta,z)=u(x,\theta)+\left(z-z_0\right)\phi_x(x,\theta),\\&u_2(x,\theta,z)=v(x,\theta)+\left(z-z_0\right)\phi_\theta(x,\theta),\\&u_3(x,\theta,z)=w(x,\theta),\end{aligned}\tag{1}$$

in which u_1, u_2 and u_3 are components of displacement along x, θ and z directions, respectively. u, v and w stand for corresponding components of displacement at neutral surface ($z=z_0$) and φ_x and φ_θ are rotation about θ and x axes, respectively. The distance of the neutral surface from the mid-surface of the shell can be calculated as [21]

$$z_0=\frac{\int_{-\frac{h}{2}}^{\frac{h}{2}} zE(z)\mathrm{d}z}{\int_{-\frac{h}{2}}^{\frac{h}{2}} E(z)\mathrm{d}z}.\tag{2}$$

and the constitutive equations can be written as follows:

$$\begin{Bmatrix}\sigma_{xx}\\\sigma_{\theta\theta}\\\sigma_{\theta z}\\\sigma_{xz}\\\sigma_{x\theta}\end{Bmatrix}=\begin{bmatrix}Q_{11}&Q_{12}&0&0&0\\Q_{21}&Q_{22}&0&0&0\\0&0&kQ_{44}&0&0\\0&0&0&kQ_{55}&0\\0&0&0&0&Q_{66}\end{bmatrix}\begin{Bmatrix}\varepsilon_{xx}\\\varepsilon_{\theta\theta}\\\gamma_{\theta z}\\\gamma_{xz}\\\gamma_{x\theta}\end{Bmatrix},\tag{4}$$

where $k=5/6$ is shear correction factor [22] and $Q_{11}-Q_{66}$ are defined as

$$\begin{aligned}&Q_{11}=Q_{22}=\frac{E}{1-\nu^2},\ Q_{12}=Q_{21}=\nu Q_{11},\\&Q_{44}=Q_{55}=Q_{66}=G=\frac{E}{2(1+\nu)}.\end{aligned}\tag{5}$$

in which E, G and ν are modulus of elasticity, shear modulus and Poisson's ratio, respectively.

The effective modulus of elasticity can be calculated using the Halpin–Tsai model as [23]

$$E=\left(\frac{3}{8}\frac{1+\xi_\mathrm{L}\eta_\mathrm{L}V_\mathrm{GNP}}{1-\eta_\mathrm{L}V_\mathrm{GNP}}+\frac{5}{8}\frac{1+\xi_\mathrm{w}\eta_\mathrm{w}V_\mathrm{GNP}}{1-\eta_\mathrm{w}V_\mathrm{GNP}}\right)E_\mathrm{m},\tag{6}$$

in which E_m is modulus of elasticity of the polymer matrix and ξ_L, ξ_w, η_L and η_w are some dimensionless parameters defined as follows:

$$\xi_L = 2\frac{l_{GNP}}{h_{GNP}},\ \xi_w = 2\frac{w_{GNP}}{h_{GNP}},\ \eta_L = \frac{\eta-1}{\eta+\xi_L},\ \eta_w = \frac{\eta-1}{\eta+\xi_w},\ \eta = \frac{E_{GNP}}{E_m}, \tag{7}$$

where E_{GNP}, l_{GNP}, w_{GNP} and h_{GNP} are modulus of elasticity, length, width and thickness of the GNPs, respectively.

In Eq. (6) V_{GNP} is volume fraction of GNPs which can be stated in terms of density of the matrix (ρ_m), density of GNPs (ρ_{GNP}) and mass fraction of GNPs (g_{GNP}) as follows:

$$V_{GNP} = \frac{g_{GNP}}{g_{GNP} + \frac{\rho_{GNP}}{\rho_m}\left(1 - g_{GNP}\right)}. \tag{8}$$

Using the rule of mixture, density and Poisson's ratio of the shell can be calculated as

$$\rho = \rho_{GNP}V_{GNP} + \rho_m V_m,\quad \nu = \nu_{GNP}V_{GNP} + \nu_m V_m, \tag{9}$$

where ν_m and ν_{GNP} are Poisson's ratio of the polymer matrix and Poisson's ratio of GNPs, respectively, and also $V_m = 1 - V_{GNP}$ is volume fraction of the matrix.

As depicted in Fig. 2, five linear types of GNPs distribution patterns are considered in this paper. Mass fraction of GNPs for these patterns can be stated as [4]

$$\begin{aligned}
&UD: && g_{GNP}(z) = g^*_{GNP},\\
&FG-A: && g_{GNP}(z) = \left(1 - \tfrac{2z}{h}\right)g^*_{GNP},\\
&FG-V: && g_{GNP}(z) = \left(1 + \tfrac{2z}{h}\right)g^*_{GNP},\\
&FG-O: && g_{GNP}(z) = 2\left(1 - \tfrac{2|z|}{h}\right)g^*_{GNP},\\
&FG-X: && g_{GNP}(z) = 4\tfrac{|z|}{h}g^*_{GNP},
\end{aligned} \tag{10}$$

in which g^*_{GNP} is total mass fraction of GNPs. It should be noted that in order to have a fair comparison between distribution patterns, Eq. (10) is regulated to have same total mass fraction of GNPs for all patterns [4].

The set of the governing equations can be derived using Hamilton's principle as [10]

$$\int_{t_1}^{t_2} \left(\delta T + \delta W_{n.c.} - \delta U_e - \delta U_h\right)dt = 0, \tag{11}$$

where $[t_1,t_2]$ is a desired time interval, δ stands for variational operator, T indicates to kinetic energy, $W_{n.c.}$ is work done by non-conservative loads, U_e stands for the strain energy of the shell and U_h indicates the strain energy generated by initial hoop tension.

The strain energy of the shell can be calculated as [24]

$$U_e = \frac{1}{2}\iiint_V \sigma_{ij}\varepsilon_{ij}dV, \tag{12}$$

in which V is volume of the shell. Using Eqs. (3) and (12) and $dV = dzdS$, the variation of the strain energy of the shell can be stated as

$$\begin{aligned}
\delta U_e = \iint_S \Bigg[& N_{xx}\frac{\partial \delta u}{\partial x} + M_{xx}\frac{\partial \delta\phi_x}{\partial x} + N_{\theta\theta}\left(\frac{\sin\alpha}{r}\delta u + \frac{1}{r}\frac{\partial\delta v}{\partial\theta} + \frac{\cos\alpha}{r}\delta w\right)\\
& + M_{\theta\theta}\left(\frac{\sin\alpha}{r}\delta\phi_x + \frac{1}{r}\frac{\partial\delta\phi_\theta}{\partial\theta}\right) + N_{x\theta}\left(\frac{1}{r}\frac{\partial\delta u}{\partial\theta} + \frac{\partial\delta v}{\partial x} - \frac{\sin\alpha}{r}\delta v\right)\\
& + M_{x\theta}\left(\frac{1}{r}\frac{\partial\delta\phi_x}{\partial\theta} + \frac{\partial\delta\phi_\theta}{\partial x} - \frac{\sin\alpha}{r}\delta\phi_\theta\right) + Q_{xz}\left(\frac{\partial\delta w}{\partial x} + \delta\phi_x\right)\\
& + Q_{\theta z}\left(-\frac{\cos\alpha}{r}\delta v + \frac{1}{r}\frac{\partial\delta w}{\partial\theta} + \delta\phi_\theta\right)\Bigg]dS,
\end{aligned} \tag{13}$$

where S is surface of the shell and stress resultant components are defined as follows:

$$\begin{Bmatrix} N_{xx}\\ N_{\theta\theta}\\ N_{x\theta}\end{Bmatrix} = \int_{-\frac{h}{2}}^{\frac{h}{2}}\begin{Bmatrix}\sigma_{xx}\\ \sigma_{\theta\theta}\\ \sigma_{x\theta}\end{Bmatrix}dz,\ \begin{Bmatrix} M_{xx}\\ M_{\theta\theta}\\ M_{x\theta}\end{Bmatrix} = \int_{-\frac{h}{2}}^{\frac{h}{2}}\begin{Bmatrix}\sigma_{xx}\\ \sigma_{\theta\theta}\\ \sigma_{x\theta}\end{Bmatrix}\left(z - z_0\right)dz,\ \begin{Bmatrix} Q_{xz}\\ Q_{\theta z}\end{Bmatrix} = \int_{-\frac{h}{2}}^{\frac{h}{2}}\begin{Bmatrix}\sigma_{xz}\\ \sigma_{\theta z}\end{Bmatrix}dz. \tag{14}$$

Substituting Eqs. (3) and (4) into Eq. (14) leads to the following relations:

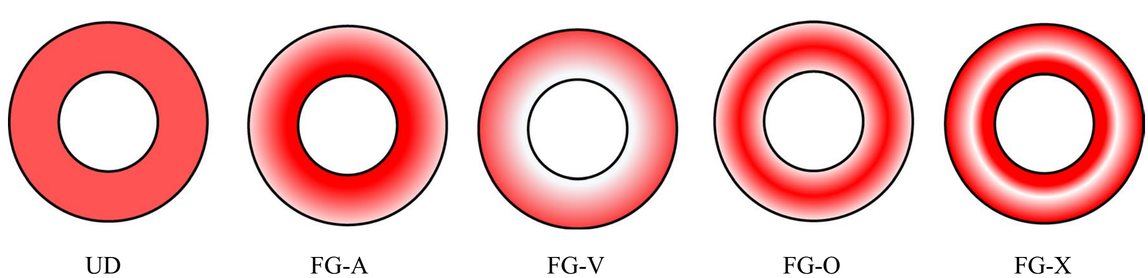

Fig. 2 GNPs distribution patterns

$$\begin{Bmatrix} N_{xx} \\ N_{\theta\theta} \\ M_{xx} \\ M_{\theta\theta} \end{Bmatrix} = \begin{bmatrix} A_{11} & B_{11} & A_{12} & B_{12} \\ A_{12} & B_{12} & A_{22} & B_{22} \\ B_{11} & D_{11} & B_{12} & D_{12} \\ B_{12} & D_{12} & B_{22} & D_{22} \end{bmatrix} \begin{Bmatrix} \frac{\partial u}{\partial x} \\ \frac{\partial \phi_x}{\partial x} \\ \frac{\sin\alpha}{r}u + \frac{1}{r}\frac{\partial v}{\partial \theta} + \frac{\cos\alpha}{r}w \\ \frac{\sin\alpha}{r}\phi_x + \frac{1}{r}\frac{\partial \phi_\theta}{\partial \theta} \end{Bmatrix}, \quad Q_{xz} = A_{55}\left(\frac{\partial w}{\partial x} + \phi_x\right),$$
$$\begin{Bmatrix} N_{x\theta} \\ M_{x\theta} \end{Bmatrix} = \begin{bmatrix} A_{66} & B_{66} \\ B_{66} & D_{66} \end{bmatrix} \begin{Bmatrix} \frac{1}{r}\frac{\partial u}{\partial \theta} + \frac{\partial v}{\partial x} - \frac{\sin\alpha}{r}v \\ \frac{1}{r}\frac{\partial \phi_x}{\partial \theta} + \frac{\partial \phi_\theta}{\partial x} - \frac{\sin\alpha}{r}\phi_\theta \end{Bmatrix}, \quad Q_{\theta z} = A_{44}\left(-\frac{\cos\alpha}{r}v + \frac{1}{r}\frac{\partial w}{\partial \theta} + \phi_\theta\right), \tag{15}$$

in which

$$\begin{Bmatrix} A_{ij} \\ B_{ij} \\ D_{ij} \end{Bmatrix} = \int_{-\frac{h}{2}}^{\frac{h}{2}} Q_{ij} \begin{Bmatrix} 1 \\ (z - z_0) \\ (z - z_0)^2 \end{Bmatrix} dz, \quad i,j = 1,2,6,$$
$$A_{ij} = k\int_{-\frac{h}{2}}^{\frac{h}{2}} Q_{ij}dz, \quad i,j = 4,5. \tag{16}$$

The strain energy created by initial hoop tension can be stated as [9, 10]

$$U_{\mathrm{h}} = \iiint_V \sigma^0_{\theta\theta}\varepsilon^{NL}_{\theta\theta}dV, \tag{17}$$

in which $\sigma^0_{\theta\theta}$ and $\varepsilon^{NL}_{\theta\theta}$ indicate initial hoop tension and non-linear part of circumferential strain which can be calculated using following relations [15, 25]:

$$\sigma^0_{\theta\theta} = \rho r^2\Omega^2,$$
$$\varepsilon^{NL}_{\theta\theta} = \frac{1}{2r^2}\left[\left(\frac{\partial u_2}{\partial \theta} + u_1\sin\alpha + u_3\cos\alpha\right)^2 + \left(\frac{\partial u_3}{\partial \theta} - u_2\cos\alpha\right)^2 + \left(\frac{\partial u_1}{\partial \theta} - u_2\sin\alpha\right)^2\right]. \tag{18}$$

Using Eqs. (1), (17) and (18) one can write

$$\begin{aligned} U_{\mathrm{h}} = \frac{\Omega^2}{2}\iint_S \Bigg\{ & I_0\Bigg[\left(\frac{\partial u}{\partial \theta}\right)^2 + \left(\frac{\partial v}{\partial \theta}\right)^2 + \left(\frac{\partial w}{\partial \theta}\right)^2 + u^2\sin^2\alpha + v^2 + w^2\cos^2\alpha + 2\left(u\frac{\partial v}{\partial \theta} - v\frac{\partial u}{\partial \theta}\right)\sin\alpha \\ & +2\left(w\frac{\partial v}{\partial \theta} - v\frac{\partial w}{\partial \theta}\right)\cos\alpha + uw\sin 2\alpha\Bigg] + 2I_1\Bigg[u\left(\frac{\partial \phi_\theta}{\partial \theta} + \phi_x\sin\alpha\right)\sin\alpha \\ & + \frac{\partial u}{\partial \theta}\left(\frac{\partial \phi_x}{\partial \theta} - \phi_\theta\sin\alpha\right) - v\left(\frac{\partial \phi_x}{\partial \theta} - \phi_\theta\sin\alpha\right)\sin\alpha + \frac{\partial v}{\partial \theta}\left(\frac{\partial \phi_\theta}{\partial \theta} + \phi_x\sin\alpha\right) \\ & +w\left(\frac{\partial \phi_\theta}{\partial \theta} + \phi_x\sin\alpha\right)\cos\alpha + \phi_\theta\left(v\cos\alpha - \frac{\partial w}{\partial \theta}\right)\cos\alpha\Bigg] \\ & +I_2\left[\left(\frac{\partial \phi_x}{\partial \theta}\right)^2 + \left(\frac{\partial \phi_\theta}{\partial \theta}\right)^2 + \phi_x^2\sin^2\alpha + \phi_\theta^2 + 2\left(\phi_x\frac{\partial \phi_\theta}{\partial \theta} - \phi_\theta\frac{\partial \phi_x}{\partial \theta}\right)\sin\alpha\right]\Bigg\}dS, \end{aligned} \tag{19}$$

in which inertia terms are defined as follows:

$$I_i = \int_{-\frac{h}{2}}^{\frac{h}{2}} (z - z_0)^i\rho(z)dz, \quad i = 0,1,2. \tag{20}$$

The kinetic energy of the shell can be calculated as

$$T = \frac{1}{2}\iiint_V \rho\vec{v}.\vec{v}dV, \tag{21}$$

in which $\vec{v}$ is absolute velocity vector and the displacement vector can be written as [13]

$$\vec{r} = u_1\vec{i} + u_2\vec{j} + u_3\vec{k}, \tag{22}$$

where u_1, u_2 and u_3 are presented based on FSDT in Eq. (1).

The absolute velocity vector can be stated using concept of relative velocity as follows [13]:

$$\vec{v} = \frac{\partial u_1}{\partial t}\vec{i} + \frac{\partial u_2}{\partial t}\vec{j} + \frac{\partial u_3}{\partial t}\vec{k} + \vec{\Omega}\times\vec{r}, \tag{23}$$

where $\vec{\Omega}$ can be stated based on Fig. 1 as follows:

$$\vec{\Omega} = \Omega\left(-\cos\alpha\vec{i} + \sin\alpha\vec{k}\right). \tag{24}$$

Substituting Eqs. (22) and (24) into Eq. (23) leads to the following equation:

$$\vec{v} = \left(\frac{\partial u_1}{\partial t} - \Omega u_2 \sin\alpha\right)\vec{i} + \left[\frac{\partial u_2}{\partial t} + \Omega\left(u_1 \sin\alpha + u_3\cos\alpha\right)\right]\vec{j} + \left(\frac{\partial u_3}{\partial t} - \Omega u_2\cos\alpha\right)\vec{k}, \tag{25}$$

and using Eqs. (1), (21) and (25) one can write

$$\begin{aligned} T = \frac{1}{2}\iint\limits_S \Bigg[& I_0\left(\frac{\partial u}{\partial t}\right)^2 + I_0\left(\frac{\partial v}{\partial t}\right)^2 + I_0\left(\frac{\partial w}{\partial t}\right)^2 + 2I_1\frac{\partial u}{\partial t}\frac{\partial \phi_x}{\partial t} \\ & + 2I_1\frac{\partial v}{\partial t}\frac{\partial \phi_\theta}{\partial t} + I_2\left(\frac{\partial \phi_x}{\partial t}\right)^2 + I_2\left(\frac{\partial \phi_\theta}{\partial t}\right)^2 + 2I_0\Omega\sin\alpha u\frac{\partial v}{\partial t} \\ & + 2I_1\Omega\sin\alpha\frac{\partial v}{\partial t}\phi_x + 2I_1\Omega\sin\alpha\frac{\partial \phi_\theta}{\partial t}u + 2I_2\Omega\sin\alpha\frac{\partial \phi_\theta}{\partial t}\phi_x \\ & + 2I_0\Omega\cos\alpha\frac{\partial v}{\partial t}w + 2I_1\Omega\cos\alpha\frac{\partial \phi_\theta}{\partial t}w - 2I_0\Omega\sin\alpha v\frac{\partial u}{\partial t} \\ & - 2I_1\Omega\sin\alpha v\frac{\partial \phi_x}{\partial t} - 2I_1\Omega\sin\alpha\phi_\theta\frac{\partial u}{\partial t} - 2I_2\Omega\sin\alpha\phi_\theta\frac{\partial \phi_x}{\partial t} \\ & - 2I_0\Omega\cos\alpha v\frac{\partial w}{\partial t} - 2I_1\Omega\cos\alpha\phi_\theta\frac{\partial w}{\partial t} + I_0\Omega^2\sin^2\alpha u^2 \\ & + I_2\Omega^2\sin^2\alpha\phi_x^2 + 2I_1\Omega^2\sin^2\alpha u\phi_x + I_0\Omega^2 v^2 + I_2\Omega^2\phi_\theta^2 + 2I_1\Omega^2 v\phi_\theta \\ & + I_0\Omega^2\cos^2\alpha w^2 + I_0\Omega^2\sin 2\alpha u w + I_1\Omega^2\sin 2\alpha w\phi_x\Bigg]\mathrm{d}S, \end{aligned} \tag{26}$$

The work done by non-conservative loads can be stated as

$$W_{\mathrm{n.c.}} = \iint\limits_S q(x,\theta)w\,\mathrm{d}S, \tag{27}$$

where q is load per unit area.

Substituting Eqs. (13), (19), (26) and (27) into Eq. (11) and using following relation for conical shells:

$$\mathrm{d}S = r(x)\mathrm{d}\theta\mathrm{d}x, \tag{28}$$

the set of the governing equations can be derived as

$$\begin{aligned} & \frac{\partial N_{xx}}{\partial x} + \frac{N_{xx} - N_{\theta\theta}}{r}\sin\alpha + \frac{1}{r}\frac{\partial N_{x\theta}}{\partial\theta} - I_0\frac{\partial^2 u}{\partial t^2} - I_1\frac{\partial^2\phi_x}{\partial t^2} + 2\Omega\left(I_0\sin\alpha\frac{\partial v}{\partial t} + I_1\sin\alpha\frac{\partial\phi_\theta}{\partial t}\right) \\ & + \Omega^2\left(I_0\frac{\partial^2 u}{\partial\theta^2} - 2I_0\sin\alpha\frac{\partial v}{\partial\theta} + I_1\frac{\partial^2\varphi_x}{\partial\theta^2} - 2I_1\sin\alpha\frac{\partial\varphi_\theta}{\partial\theta}\right) = 0, \\ & \frac{1}{r}\frac{\partial N_{\theta\theta}}{\partial\theta} + 2\frac{N_{x\theta}}{r}\sin\alpha + \frac{Q_{\theta z}}{r}\cos\alpha + \frac{\partial N_{x\theta}}{\partial x} - I_0\frac{\partial^2 v}{\partial t^2} - I_1\frac{\partial^2\phi_\theta}{\partial t^2} - 2\Omega\left(I_0\sin\alpha\frac{\partial u}{\partial t} + I_0\cos\alpha\frac{\partial w}{\partial t} + I_1\sin\alpha\frac{\partial\phi_x}{\partial t}\right) + \Omega^2\Bigg(2I_0\sin\alpha\frac{\partial u}{\partial\theta} \\ & + I_0\frac{\partial^2 v}{\partial\theta^2} + 2I_0\cos\alpha\frac{\partial w}{\partial\theta} + 2I_1\sin\alpha\frac{\partial\varphi_x}{\partial\theta} + I_1\frac{\partial^2\varphi_\theta}{\partial\theta^2}\Bigg) = 0, -\frac{N_{\theta\theta}}{r}\cos\alpha + \frac{\partial Q_{xz}}{\partial x} + \frac{Q_{xz}}{r}\sin\alpha + \frac{1}{r}\frac{\partial Q_{\theta z}}{\partial\theta} - I_0\frac{\partial^2 w}{\partial t^2} \\ & + 2\Omega\left(I_0\cos\alpha\frac{\partial v}{\partial t} + I_1\cos\alpha\frac{\partial\phi_\theta}{\partial t}\right) + \Omega^2\left(-2I_0\cos\alpha\frac{\partial v}{\partial\theta} + I_0\frac{\partial^2 w}{\partial\theta^2} - 2I_1\cos\alpha\frac{\partial\varphi_\theta}{\partial\theta}\right) = -q, \frac{\partial M_{xx}}{\partial x} + \frac{M_{xx} - M_{\theta\theta}}{r}\sin\alpha \\ & + \frac{1}{r}\frac{\partial M_{x\theta}}{\partial\theta} - Q_{xz} - I_1\frac{\partial^2 u}{\partial t^2} - I_2\frac{\partial^2\phi_x}{\partial t^2} + 2\Omega\left(I_1\sin\alpha\frac{\partial v}{\partial t} + I_2\sin\alpha\frac{\partial\phi_\theta}{\partial t}\right) + \Omega^2\left(I_1\frac{\partial^2 u}{\partial\theta^2} - 2I_1\sin\alpha\frac{\partial v}{\partial\theta} + I_2\frac{\partial^2\varphi_x}{\partial\theta^2} - 2I_2\sin\alpha\frac{\partial\varphi_\theta}{\partial\theta}\right) = 0, \\ & \frac{1}{r}\frac{\partial M_{\theta\theta}}{\partial\theta} + \frac{\partial M_{x\theta}}{\partial x} + 2\frac{M_{x\theta}}{r}\sin\alpha - Q_{\theta z} - I_1\frac{\partial^2 v}{\partial t^2} - I_2\frac{\partial^2\phi_\theta}{\partial t^2} - 2\Omega\left(I_1\sin\alpha\frac{\partial u}{\partial t} + I_1\cos\alpha\frac{\partial w}{\partial t} + I_2\sin\alpha\frac{\partial\phi_x}{\partial t}\right) + \Omega^2\Bigg(2I_1\sin\alpha\frac{\partial u}{\partial\theta} \\ & + I_1\frac{\partial^2 v}{\partial\theta^2} + 2I_1\cos\alpha\frac{\partial w}{\partial\theta} + 2I_2\sin\alpha\frac{\partial\varphi_x}{\partial\theta} + I_2\frac{\partial^2\varphi_\theta}{\partial\theta^2}\Bigg) = 0. \end{aligned} \tag{29}$$

and the boundary conditions can be written as follows:

$$\begin{aligned} \text{Clamped}\,(C): &\quad u = 0, \quad v = 0, \quad w = 0, \quad \phi_x = 0, \quad \phi_\theta = 0, \\ \text{Simply Supported}\,(S): &\quad N_{xx} = 0, \quad v = 0, \quad w = 0, \quad M_{xx} = 0, \quad \phi_\theta = 0, \\ \text{Free}\,(F): &\quad N_{xx} = 0, \; N_{x\theta} = 0, \; Q_{xz} = 0, \; M_{xx} = 0, \; M_{x\theta} = 0. \end{aligned} \tag{30}$$

Substituting Eq. (15) into Eq. (29), the set of the governing equations can be written for free vibration analysis ($q=0$) as follows:

$$
\begin{aligned}
&A_{11}\frac{\partial^2 u}{\partial x^2}+\frac{A_{11}\sin\alpha}{r}\frac{\partial u}{\partial x}+\left(\frac{A_{66}}{r^2}+I_0\Omega^2\right)\frac{\partial^2 u}{\partial\theta^2}-\frac{A_{22}\sin^2\alpha}{r^2}u\\
&\quad+\frac{A_{12}+A_{66}}{r}\frac{\partial^2 v}{\partial x\partial\theta}-\sin\alpha\left(\frac{A_{22}+A_{66}}{r^2}+2I_0\Omega^2\right)\frac{\partial v}{\partial\theta}+\frac{A_{12}\cos\alpha}{r}\frac{\partial w}{\partial x}\\
&\quad-\frac{A_{22}\sin 2\alpha}{2r^2}w+B_{11}\frac{\partial^2\phi_x}{\partial x^2}+\frac{B_{11}\sin\alpha}{r}\frac{\partial\phi_x}{\partial x}+\left(\frac{B_{66}}{r^2}+I_1\Omega^2\right)\frac{\partial^2\varphi_x}{\partial\theta^2}\\
&\quad-\frac{B_{22}\sin^2\alpha}{r^2}\phi_x+\frac{B_{12}+B_{66}}{r}\frac{\partial^2\phi_\theta}{\partial x\partial\theta}-\sin\alpha\left(\frac{B_{22}+B_{66}}{r^2}+2I_1\Omega^2\right)\frac{\partial\varphi_\theta}{\partial\theta}\\
&\quad+2\Omega I_0\sin\alpha\frac{\partial v}{\partial t}+2\Omega I_1\sin\alpha\frac{\partial\phi_\theta}{\partial t}-I_0\frac{\partial^2 u}{\partial t^2}-I_1\frac{\partial^2\phi_x}{\partial t^2}=0,\\
&\frac{A_{12}+A_{66}}{r}\frac{\partial^2 u}{\partial x\partial\theta}+\sin\alpha\left(\frac{A_{22}+A_{66}}{r^2}+2I_0\Omega^2\right)\frac{\partial u}{\partial\theta}+A_{66}\frac{\partial^2 v}{\partial x^2}\\
&\quad+\frac{A_{66}\sin\alpha}{r}\frac{\partial v}{\partial x}+\left(\frac{A_{22}}{r^2}+I_0\Omega^2\right)\frac{\partial^2 v}{\partial\theta^2}-\frac{A_{44}\cos^2\alpha+A_{66}\sin^2\alpha}{r^2}v\\
&\quad+\cos\alpha\left(\frac{A_{22}+A_{44}}{r^2}+2I_0\Omega^2\right)\frac{\partial w}{\partial\theta}+\frac{B_{12}+B_{66}}{r}\frac{\partial^2\phi_x}{\partial x\partial\theta}+\sin\alpha\\
&\quad\left(\frac{B_{22}+B_{66}}{r^2}+2I_1\Omega^2\right)\frac{\partial\varphi_x}{\partial\theta}+B_{66}\frac{\partial^2\phi_\theta}{\partial x^2}+\frac{B_{66}\sin\alpha}{r}\frac{\partial\phi_\theta}{\partial x}\\
&\quad+\left(\frac{B_{22}}{r^2}+I_1\Omega^2\right)\frac{\partial^2\varphi_\theta}{\partial\theta^2}+\left(\frac{A_{44}\cos\alpha}{r}-\frac{B_{66}\sin^2\alpha}{r^2}\right)\phi_\theta-2I_0\Omega\sin\\
&\quad\alpha\frac{\partial u}{\partial t}-2I_0\Omega\cos\alpha\frac{\partial w}{\partial t}-2I_1\Omega\sin\alpha\frac{\partial\phi_x}{\partial t}-I_0\frac{\partial^2 v}{\partial t^2}-I_1\frac{\partial^2\phi_\theta}{\partial t^2}=0,\\
&-\frac{A_{12}\cos\alpha}{r}\frac{\partial u}{\partial x}-\frac{A_{22}\sin 2\alpha}{2r^2}u-\cos\alpha\left(\frac{A_{22}+A_{44}}{r^2}+2I_0\Omega^2\right)\\
&\quad\frac{\partial v}{\partial\theta}+A_{55}\frac{\partial^2 w}{\partial x^2}+\frac{A_{55}\sin\alpha}{r}\frac{\partial w}{\partial x}+\left(\frac{A_{44}}{r^2}+I_0\Omega^2\right)\frac{\partial^2 w}{\partial\theta^2}-\frac{A_{22}\cos^2\alpha}{r^2}w\\
&\quad+\left(A_{55}-\frac{B_{12}\cos\alpha}{r}\right)\frac{\partial\phi_x}{\partial x}+\left(\frac{A_{55}\sin\alpha}{r}-\frac{B_{22}\sin 2\alpha}{2r^2}\right)\phi_x+\left[\frac{A_{44}}{r}-\left(\frac{B_{22}}{r^2}\right.\right.\\
&\quad\left.\left.+2I_1\Omega^2\right)\cos\alpha\right]\frac{\partial\phi_\theta}{\partial\theta}+2I_0\Omega\cos\alpha\frac{\partial v}{\partial t}+2I_1\Omega\cos\alpha\frac{\partial\phi_\theta}{\partial t}-I_0\frac{\partial^2 w}{\partial t^2}=0,\\
&B_{11}\frac{\partial^2 u}{\partial x^2}+\frac{B_{11}\sin\alpha}{r}\frac{\partial u}{\partial x}+\left(\frac{B_{66}}{r^2}+I_1\Omega^2\right)\frac{\partial^2 u}{\partial\theta^2}-\frac{B_{22}\sin^2\alpha}{r^2}u\\
&\quad+\frac{B_{12}+B_{66}}{r}\frac{\partial^2 v}{\partial x\partial\theta}-\sin\alpha\left(\frac{B_{22}+B_{66}}{r^2}+2I_1\Omega^2\right)\frac{\partial v}{\partial\theta}-\left(A_{55}-\frac{B_{12}\cos\alpha}{r}\right)\frac{\partial w}{\partial x}\\
&\quad-\frac{B_{22}\sin 2\alpha}{2r^2}w+D_{11}\frac{\partial^2\phi_x}{\partial x^2}+\frac{D_{11}\sin\alpha}{r}\frac{\partial\phi_x}{\partial x}+\left(\frac{D_{66}}{r^2}+I_2\Omega^2\right)\frac{\partial^2\varphi_x}{\partial\theta^2}\\
&\quad-\left(A_{55}+\frac{D_{22}\sin^2\alpha}{r^2}\right)\phi_x+\frac{D_{12}+D_{66}}{r}\frac{\partial^2\phi_\theta}{\partial x\partial\theta}-\sin\alpha\left(\frac{D_{22}+D_{66}}{r^2}+2I_2\Omega^2\right)\\
&\quad\frac{\partial\varphi_\theta}{\partial\theta}+2I_1\Omega\sin\alpha\frac{\partial v}{\partial t}+2I_2\Omega\sin\alpha\frac{\partial\phi_\theta}{\partial t}-I_1\frac{\partial^2 u}{\partial t^2}-I_2\frac{\partial^2\phi_x}{\partial t^2}=0,\\
&\frac{B_{12}+B_{66}}{r}\frac{\partial^2 u}{\partial x\partial\theta}+\sin\alpha\left(\frac{B_{22}+B_{66}}{r^2}+2I_1\Omega^2\right)\frac{\partial u}{\partial\theta}+B_{66}\frac{\partial^2 v}{\partial x^2}\\
&\quad+\frac{B_{66}\sin\alpha}{r}\frac{\partial v}{\partial x}+\left(\frac{B_{22}}{r^2}+I_1\Omega^2\right)\frac{\partial^2 v}{\partial\theta^2}+\left(\frac{A_{44}\cos\alpha}{r}-\frac{B_{66}\sin^2\alpha}{r^2}\right)v\\
&\quad+\left[-\frac{A_{44}}{r}+\left(\frac{B_{22}}{r^2}+2I_1\Omega^2\right)\cos\alpha\right]\frac{\partial w}{\partial\theta}+\frac{D_{12}+D_{66}}{r}\frac{\partial^2\phi_x}{\partial x\partial\theta}\\
&\quad+\sin\alpha\left(\frac{D_{22}+D_{66}}{r^2}+2I_2\Omega^2\right)\frac{\partial\varphi_x}{\partial\theta}+D_{66}\frac{\partial^2\phi_\theta}{\partial x^2}+\frac{D_{66}\sin\alpha}{r}\frac{\partial\phi_\theta}{\partial x}\\
&\quad+\left(\frac{D_{22}}{r^2}+I_2\Omega^2\right)\frac{\partial^2\varphi_\theta}{\partial\theta^2}-\left(A_{44}+\frac{D_{66}\sin^2\alpha}{r^2}\right)\phi_\theta-2I_1\Omega\sin\alpha\frac{\partial u}{\partial t}\\
&\quad-2I_1\Omega\cos\alpha\frac{\partial w}{\partial t}-2I_2\Omega\sin\alpha\frac{\partial\phi_x}{\partial t}-I_1\frac{\partial^2 v}{\partial t^2}-I_2\frac{\partial^2\phi_\theta}{\partial t^2}=0.
\end{aligned}
\tag{31}
$$

It is worth mentioning that in Eq. (31), the terms containing second time derivatives of displacements are relative acceleration, the terms containing square of rotational speed denote the centrifugal acceleration along with initial hoop tension and the terms containing rotational speed and first time derivatives of displacements are Coriolis parts of acceleration.

In a similar manner, by substituting Eq. (15) into Eq. (30) and doing some simplifications for simply supported condition, the boundary conditions can be written as follows:

$$
\begin{aligned}
&\text{Clamped}\,(C):\quad u=0,\ v=0,\ w=0,\ \phi_x=0,\ \phi_\theta=0,\\
&\text{Simply Supported}\,(S):\quad A_{11}\frac{\partial u}{\partial x}+\frac{A_{12}\sin\alpha}{r}u+B_{11}\frac{\partial\phi_x}{\partial x}\\
&+\frac{B_{12}\sin\alpha}{r}\phi_x=0, v=0,\\
&w=0,\ B_{11}\frac{\partial u}{\partial x}+\frac{B_{12}\sin\alpha}{r}u+D_{11}\frac{\partial\phi_x}{\partial x}\\
&+\frac{D_{12}\sin\alpha}{r}\phi_x=0,\ \phi_\theta=0,\\
&\text{Free}\,(F):\\
&A_{11}\frac{\partial u}{\partial x}+B_{11}\frac{\partial\phi_x}{\partial x}+A_{12}\left(\frac{\sin\alpha}{r}u+\frac{1}{r}\frac{\partial v}{\partial\theta}+\frac{\cos\alpha}{r}w\right)\\
&+B_{12}\left(\frac{\sin\alpha}{r}\phi_x+\frac{1}{r}\frac{\partial\phi_\theta}{\partial\theta}\right)=0,\\
&A_{66}\left(\frac{1}{r}\frac{\partial u}{\partial\theta}+\frac{\partial v}{\partial x}-\frac{\sin\alpha}{r}v\right)\\
&+B_{66}\left(\frac{1}{r}\frac{\partial\phi_x}{\partial\theta}+\frac{\partial\phi_\theta}{\partial x}-\frac{\sin\alpha}{r}\phi_\theta\right)=0,\\
&\frac{\partial w}{\partial x}+\phi_x=0,\\
&B_{11}\frac{\partial u}{\partial x}+D_{11}\frac{\partial\phi_x}{\partial x}+B_{12}\left(\frac{\sin\alpha}{r}u+\frac{1}{r}\frac{\partial v}{\partial\theta}+\frac{\cos\alpha}{r}w\right)\\
&+D_{12}\left(\frac{\sin\alpha}{r}\phi_x+\frac{1}{r}\frac{\partial\phi_\theta}{\partial\theta}\right)=0,\\
&B_{66}\left(\frac{1}{r}\frac{\partial u}{\partial\theta}+\frac{\partial v}{\partial x}-\frac{\sin\alpha}{r}v\right)\\
&+D_{66}\left(\frac{1}{r}\frac{\partial\phi_x}{\partial\theta}+\frac{\partial\phi_\theta}{\partial x}-\frac{\sin\alpha}{r}\phi_\theta\right)=0.
\end{aligned}
\tag{32}
$$

Using the following solution [25]:

$$
\begin{Bmatrix} u(x,\theta,t)\\ v(x,\theta,t)\\ w(x,\theta,t)\\ \phi_x(x,\theta,t)\\ \phi_\theta(x,\theta,t)\end{Bmatrix}=\begin{Bmatrix} U(x)\cos(n\theta+\omega t)\\ V(x)\sin(n\theta+\omega t)\\ W(x)\cos(n\theta+\omega t)\\ X(x)\cos(n\theta+\omega t)\\ \Theta(x)\sin(n\theta+\omega t)\end{Bmatrix},\ n=1,2,3,\ldots,
\tag{33}
$$

in which ω is natural frequency and n is circumferential mode number, Eq. (31) can be written as follows:

$$
\begin{aligned}
&A_{11}U'' + \frac{A_{11}\sin\alpha}{r}U' - \left(\frac{A_{22}\sin^2\alpha + A_{66}n^2}{r^2} + n^2 I_0\Omega^2\right)U + \frac{n(A_{12}+A_{66})}{r}V' - n\sin\alpha\left(\frac{A_{22}+A_{66}}{r^2} + 2I_0\Omega^2\right)V \\
&+ \frac{A_{12}\cos\alpha}{r}W' - \frac{A_{22}\sin 2\alpha}{2r^2}W + B_{11}X'' + \frac{B_{11}\sin\alpha}{r}X' - \left(\frac{B_{22}\sin^2\alpha + B_{66}n^2}{r^2} + n^2 I_1\Omega^2\right)X \\
&+ \frac{n(B_{12}+B_{66})}{r}\Theta' - n\sin\alpha\left(\frac{B_{22}+B_{66}}{r^2} + 2I_1\Omega^2\right)\Theta + 2\Omega\omega I_0\sin\alpha V + 2\Omega\omega I_1\sin\alpha\Theta + I_0\omega^2 U + I_1\omega^2 X = 0, \\
&-\frac{n(A_{12}+A_{66})}{r}U' - n\sin\alpha\left(\frac{A_{22}+A_{66}}{r^2} + 2I_0\Omega^2\right)U + A_{66}V'' + \frac{A_{66}\sin\alpha}{r}V' \\
&-\left(\frac{A_{22}n^2 + A_{44}\cos^2\alpha + A_{66}\sin^2\alpha}{r^2} + n^2 I_0\Omega^2\right)V - n\cos\alpha\left(\frac{A_{22}+A_{44}}{r^2} + 2I_0\Omega^2\right)W \\
&\quad -\frac{n(B_{12}+B_{66})}{r}X' - n\sin\alpha\left(\frac{B_{22}+B_{66}}{r^2} + 2I_1\Omega^2\right)X + B_{66}\Theta'' + \frac{B_{66}\sin\alpha}{r}\Theta' \\
&\quad +\left(\frac{A_{44}\cos\alpha}{r} - \frac{B_{22}n^2 + B_{66}\sin^2\alpha}{r^2} - n^2 I_1\Omega^2\right)\Theta + 2I_0\Omega\omega\sin\alpha U + 2I_0\Omega\omega\cos\alpha W \\
&\quad + 2I_1\Omega\omega\sin\alpha X + I_0\omega^2 V + I_1\omega^2\Theta = 0, \\
&-\frac{A_{12}\cos\alpha}{r}U' - \frac{A_{22}\sin 2\alpha}{2r^2}U - n\cos\alpha\left(\frac{A_{22}+A_{44}}{r^2} + 2I_0\Omega^2\right)V + A_{55}W'' + \frac{A_{55}\sin\alpha}{r}W' \\
&\quad -\left(\frac{A_{22}\cos^2\alpha + A_{44}n^2}{r^2} + n^2 I_0\Omega^2\right)W + \left(A_{55} - \frac{B_{12}\cos\alpha}{r}\right)X' + \left(\frac{A_{55}\sin\alpha}{r} - \frac{B_{22}\sin 2\alpha}{2r^2}\right)X \\
&\quad + n\left[\frac{A_{44}}{r} - \left(\frac{B_{22}}{r^2} + 2I_1\Omega^2\right)\cos\alpha\right]\Theta + 2I_0\Omega\omega\cos\alpha V + 2I_1\Omega\omega\cos\alpha\Theta + I_0\omega^2 W = 0, \\
&B_{11}U'' + \frac{B_{11}\sin\alpha}{r}U' - \left(\frac{B_{22}\sin^2\alpha + B_{66}n^2}{r^2} + n^2 I_1\Omega^2\right)U + \frac{n(B_{12}+B_{66})}{r}V' \\
&\quad - n\sin\alpha\left(\frac{B_{22}+B_{66}}{r^2} + 2I_1\Omega^2\right)V - \left(A_{55} - \frac{B_{12}\cos\alpha}{r}\right)W' - \frac{B_{22}\sin 2\alpha}{2r^2}W \\
&\quad + D_{11}X'' + \frac{D_{11}\sin\alpha}{r}X' - \left(\frac{D_{22}\sin^2\alpha + D_{66}n^2}{r^2} + A_{55} + n^2 I_2\Omega^2\right)X \\
&\quad + \frac{n(D_{12}+D_{66})}{r}\Theta' - n\sin\alpha\left(\frac{D_{22}+D_{66}}{r^2} + 2I_2\Omega^2\right)\Theta + 2I_1\Omega\omega\sin\alpha V \\
&\quad + 2I_2\Omega\omega\sin\alpha\Theta + I_1\omega^2 U + I_2\omega^2 X = 0, \\
&-\frac{n(B_{12}+B_{66})}{r}U' - n\sin\alpha\left(\frac{B_{22}+B_{66}}{r^2} + 2I_1\Omega^2\right)U + B_{66}V'' + \frac{B_{66}\sin\alpha}{r}V' + \left(\frac{A_{44}\cos\alpha}{r} - \frac{B_{22}n^2 + B_{66}\sin^2\alpha}{r^2} - n^2 I_1\Omega^2\right)V + n\left[\frac{A_{44}}{r} - \left(\frac{B_{22}}{r^2} + 2I_1\Omega^2\right)\cos\alpha\right]W \\
&\quad -\frac{n(D_{12}+D_{66})}{r}X' - n\sin\alpha\left(\frac{D_{22}+D_{66}}{r^2} + 2I_2\Omega^2\right)X + D_{66}\Theta'' + \frac{D_{66}\sin\alpha}{r}\Theta' - \left(\frac{D_{22}n^2 + D_{66}\sin^2\alpha}{r^2} + A_{44} + n^2 I_2\Omega^2\right)\Theta + 2I_1\Omega\omega\sin\alpha U + 2I_1\Omega\omega\cos\alpha W \\
&\quad + 2I_2\Omega\omega\sin\alpha X + I_1\omega^2 V + I_2\omega^2\Theta = 0.
\end{aligned} \tag{34}
$$

in which prime denotes derivative with respect the spatial variable x. In a similar manner, using Eqs. (32) and (33), the boundary conditions can be written as follows:

$$
\begin{aligned}
&\text{Clamped}\,(C):\quad U = 0,\ V = 0,\ W = 0,\ X = 0,\ \Theta = 0, \\
&\text{Simply Supported}\,(S):\quad A_{11}U' + \frac{A_{12}\sin\alpha}{r}U + B_{11}X' + \frac{B_{12}\sin\alpha}{r}X = 0,\ V = 0, \\
&W = 0,\ B_{11}U' + \frac{B_{12}\sin\alpha}{r}U + D_{11}X' + \frac{D_{12}\sin\alpha}{r}X = 0,\ \Theta = 0, \\
&\text{Free}\,(F): \\
&A_{11}U' + B_{11}X' + \frac{A_{12}}{r}(\sin\alpha U + nV + \cos\alpha W) + \frac{B_{12}}{r}(\sin\alpha X + n\Theta) = 0, \\
&A_{66}\left(-\frac{n}{r}U + V' - \frac{\sin\alpha}{r}V\right) + B_{66}\left(-\frac{n}{r}X + \Theta' - \frac{\sin\alpha}{r}\Theta\right) = 0, \\
&W' + X = 0, \\
&B_{11}U' + D_{11}X' + \frac{B_{12}}{r}(\sin\alpha U + nV + \cos\alpha W) + \frac{D_{12}}{r}(\sin\alpha X + n\Theta) = 0, \\
&B_{66}\left(-\frac{n}{r}U + V' - \frac{\sin\alpha}{r}V\right) + D_{66}\left(-\frac{n}{r}X + \Theta' - \frac{\sin\alpha}{r}\Theta\right) = 0.
\end{aligned} \tag{35}
$$

3 Solution procedure

Due to the mathematical complexities in the set of the governing equations and boundary conditions, a numerical solution is presented here using DQM. This method is based on this idea that all derivatives of a function like $f(x)$ can be estimated by means of the weighted linear sum of the values of the function at N pre-selected grid of discrete points as [26]

$$\left.\frac{\mathrm{d}^r f}{\mathrm{d}x^r}\right|_{x=x_i} = \sum_{j=1}^{N} A_{ij}^{(r)} f_j, \tag{36}$$

in which $[\mathbf{A}^{(\mathbf{r})}]$ is the weighting coefficient associated with the rth order derivative which can be calculated as follows [26]:

$$A_{ij}^{(1)} = \begin{cases} \dfrac{\prod\limits_{\substack{m=1\\ m\neq i,j}}^{N} \left(x_i - x_m\right)}{\prod\limits_{\substack{m=1\\ m\neq j}}^{N} \left(x_j - x_m\right)}, & i,j = 1,2,3,\ldots,N;\ i \neq j \\ \sum\limits_{\substack{m=1\\ m\neq i}}^{N} \dfrac{1}{x_i - x_m}, & i = j = 1,2,3,\ldots,N \end{cases}, \tag{37}$$

$$A^{(r)} = A^{(1)} A^{(r-1)}, \quad r = 2,3,\ldots,N-1.$$

Distribution of grid points plays an important role in convergence of the solution using DQM. A well-accepted set of the grid points is the Gauss–Lobatto–Chebyshev points given for $0 \leq x \leq L$ as [26]

Table 1 Convergence of the presented numerical solution

n		m	$N=7$	$N=9$	$N=11$	$N=13$	$N=15$	$N=17$
1	Forward	1	2422.953	2412.233	2410.593	2410.094	2410.114	2410.136
		2	2504.059	2497.010	2500.215	2500.862	2500.935	2500.933
		3	3286.674	3227.666	3232.732	3231.327	3231.360	3231.392
	Backward	1	1477.263	1474.638	1473.746	1473.369	1473.329	1473.336
		2	2466.686	2453.447	2454.354	2454.527	2454.630	2454.651
		3	3009.080	2996.514	3000.600	3000.722	3000.851	3000.863
2	Forward	1	1656.612	1658.607	1658.802	1658.450	1658.327	1658.308
		2	2660.994	2653.639	2653.333	2652.927	2652.931	2652.952
		3	3405.157	3325.211	3328.189	3326.099	3326.110	3326.094
	Backward	1	916.0765	918.3045	918.4430	918.0316	917.8874	917.8670
		2	2167.852	2165.257	2164.561	2164.396	2164.428	2164.450
		3	2998.231	3002.118	3004.497	3003.189	3003.199	3003.164
3	Forward	1	1795.408	1797.626	1798.355	1798.372	1798.324	1798.307
		2	2523.495	2521.542	2520.798	2520.593	2520.589	2520.607
		3	3231.620	3244.472	3244.771	3244.139	3244.225	3244.196
	Backward	1	1254.819	1257.236	1258.011	1258.020	1257.963	1257.943
		2	2069.890	2068.378	2067.492	2067.379	2067.399	2067.421
		3	2855.313	2909.961	2909.752	2909.665	2909.716	2909.677
4	Forward	1	2308.748	2309.476	2309.895	2309.981	2309.986	2309.983
		2	2829.753	2829.231	2828.473	2828.221	2828.181	2828.187
		3	3502.518	3490.283	3485.355	3484.840	3485.014	3484.996
	Backward	1	1905.402	1906.145	1906.599	1906.692	1906.697	1906.692
		2	2467.951	2467.924	2466.841	2466.619	2466.585	2466.594
		3	3175.574	3190.013	3184.416	3184.319	3184.474	3184.448

Table 2 Dimensionless natural frequencies of a CC stationary homogenous truncated conical shell ($\nu=0.3$, $\alpha=45°$, $h/b=0.01$, $L\sin\alpha/b=0.5$, $m=1$)

n	1	2	3	4	5	6	7	8	9
Present	0.8117	0.6694	0.5426	0.4563	0.4085	0.3957	0.4134	0.4556	0.5160
Liew et al. [36]	0.8120	0.6696	0.5428	0.4565	0.4088	0.3961	0.4141	0.4567	0.5175
Shu [37]	0.8120	0.6696	0.5428	0.4566	0.4089	0.3963	0.4143	0.4568	0.5177

Table 3 Dimensionless forward and backward frequencies of a rotating homogenous truncated conical shell ($\nu=0.3$, $\alpha=30°$, $h/a=0.01$, $L/a=6$, $n=m=1$)

	$\Omega^*=0.2$		$\Omega^*=0.3$	
	Forward	Backward	Forward	Backward
CC				
Present	0.8852	0.5990	0.9432	0.5198
Dai et al. [32]	0.8836	0.6018	0.9260	0.5265
SC				
Present	0.8797	0.5941	0.9407	0.5160
Dai et al. [32]	0.8784	0.5963	0.9254	0.5215
CS				
Present	0.7587	0.5420	0.7918	0.4504
Dai et al. [32]	0.7642	0.5357	0.8030	0.4369
SS				
Present	0.7210	0.5388	0.7555	0.4479
Dai et al. [32]	0.7290	0.5331	0.7724	0.4350

$$x_i = \frac{L}{2}\left\{1 - \cos\left[\frac{(i-1)\pi}{N-1}\right]\right\}, \quad i = 1, 2, 3, \ldots, N. \tag{38}$$

Using the following notation:

$$[A] = \left[A^{(1)}\right],\ [B] = \left[A^{(2)}\right], \tag{39}$$

Equation (36) can be rewritten for the first two derivates as

$$\left\{\frac{\mathrm{d}f}{\mathrm{d}x}\right\} = [A]\{f\},\ \left\{\frac{\mathrm{d}^2 f}{\mathrm{d}x^2}\right\} = [B]\{f\}. \tag{40}$$

Applying Eq. (40), the set of the governing Eq. (34) can be written in the following algebraic form:

$$\omega^2[M]\{s\} + \omega[G]\{s\} + [K]\{s\} = \{0\}, \tag{41}$$

where **[M]**, **[G]**, **[K]** and $\{s\}$ are mass matrix, gyroscopic matrix, stiffness matrix and displacement vector which are presented in details in Appendix A.

Using Eqs. (35) and (40), the boundary conditions can be written in the following algebraic form:

$$[T]\{s\} = \{0\}, \tag{42}$$

in which matrix **[T]** is presented in Appendix B for various boundary conditions.

Simultaneous solution of algebraic Eqs. (41) and (42) leads to inconsistency between number of unknown variables and number of equations. In order to overcome this challenge, let us divide the grid points into two sets: boundary points (x_1 and x_N) and domain ones ($x_2 - x_{N-1}$). By neglecting satisfying Eq. (41) at the boundary points, this equation can be written as

$$\omega^2\left[\bar{M}\right]\{s\} + \omega\left[\bar{G}\right]\{s\} + \left[\bar{K}\right]\{s\} = \{0\}, \tag{43}$$

in which bar sign implies the corresponding non-square matrix. Equations (42) and (43) can be rearranged and partitioned in order to separate the boundary and domain points as follows:

$$\begin{aligned}&\omega^2\left(\left[\bar{M}\right]_{\mathrm{b}}\{s\}_{\mathrm{b}} + \left[\bar{M}\right]_{\mathrm{d}}\{s\}_{\mathrm{d}}\right) + \omega\left(\left[\bar{G}\right]_{\mathrm{b}}\{s\}_{\mathrm{b}} + \left[\bar{G}\right]_{\mathrm{d}}\{s\}_{\mathrm{d}}\right)\\ &\quad + \left[\bar{K}\right]_{\mathrm{b}}\{s\}_{\mathrm{b}} + \left[\bar{K}\right]_{\mathrm{d}}\{s\}_{\mathrm{d}} = \{0\},\end{aligned} \tag{44-a}$$

$$[T]_{\mathrm{d}}\{s\}_{\mathrm{d}} + [T]_{\mathrm{b}}\{s\}_{\mathrm{b}} = \{0\}, \tag{44-b}$$

where subscripts "b" and "d" indicate to boundary and domain points, respectively. Substituting Eq. (44-b) into Eq. (44-a) leads to the following eigen value equation:

$$\omega^2\left[M^*\right]\{s\}_{\mathrm{d}} + \omega\left[G^*\right]\{s\}_{\mathrm{d}} + \left[K^*\right]\{s\}_{\mathrm{d}} = \{0\}, \tag{45}$$

in which

$$\begin{aligned}&\left[M^*\right] = \left[\bar{M}\right]_d + \left[\bar{M}\right]_b[p],\quad \left[K^*\right] = \left[\bar{K}\right]_d + \left[\bar{K}\right]_b[p],\\ &\left[G^*\right] = \left[\bar{G}\right]_d + \left[\bar{G}\right]_b[p],\quad [p] = -[T]_b^{-1}[T]_d.\end{aligned} \tag{46}$$

The eigenvalue Eq. (45) provides the natural frequencies of the rotating conical shells. Among all these frequencies, there are two sets of natural frequencies, the positive values which are known as forward frequencies and negative ones which are known as backward frequencies [27–31]. It is worth mentioning that the reverse definition is used by some authors as well [25, 32].

4 Numerical results

Numerical results are provided in this section to confirm convergence and accuracy of the presented numerical solution and examine the influences of different parameters on the forward and backward frequencies of rotating GNP-reinforced truncated conical shells. Except for the cases which are mentioned directly, in what follows, material properties of the epoxy and GNPs are considered as $E_{\mathrm{m}}=3$ GPa, $\nu_{\mathrm{m}}=0.34$, $\rho_{\mathrm{m}}=1200$ kg/m^3, $E_{\mathrm{GNP}}=1.01$ TPa, $\nu_{\mathrm{GNP}}=0.186$ and $\rho_{\mathrm{GNP}}=1060$ kg/m^3 [33–35] and results are presented for a rotating GNP-reinforced truncated conical shell clamped at $x=0$ and simply supported at $x=L$ (CS). The shell is of $a=0.5$ m, $\alpha=20°$, $L/a=4$, $h/a=0.1$ which is rotating at $\Omega=500$ rad/s and FG-A distribution pattern is chosen for GNPs of $g^*_{\mathrm{GNP}}=0.01$, $l_{\mathrm{GNP}}/a=2\times10^{-6}$, $w_{\mathrm{GNP}}/$

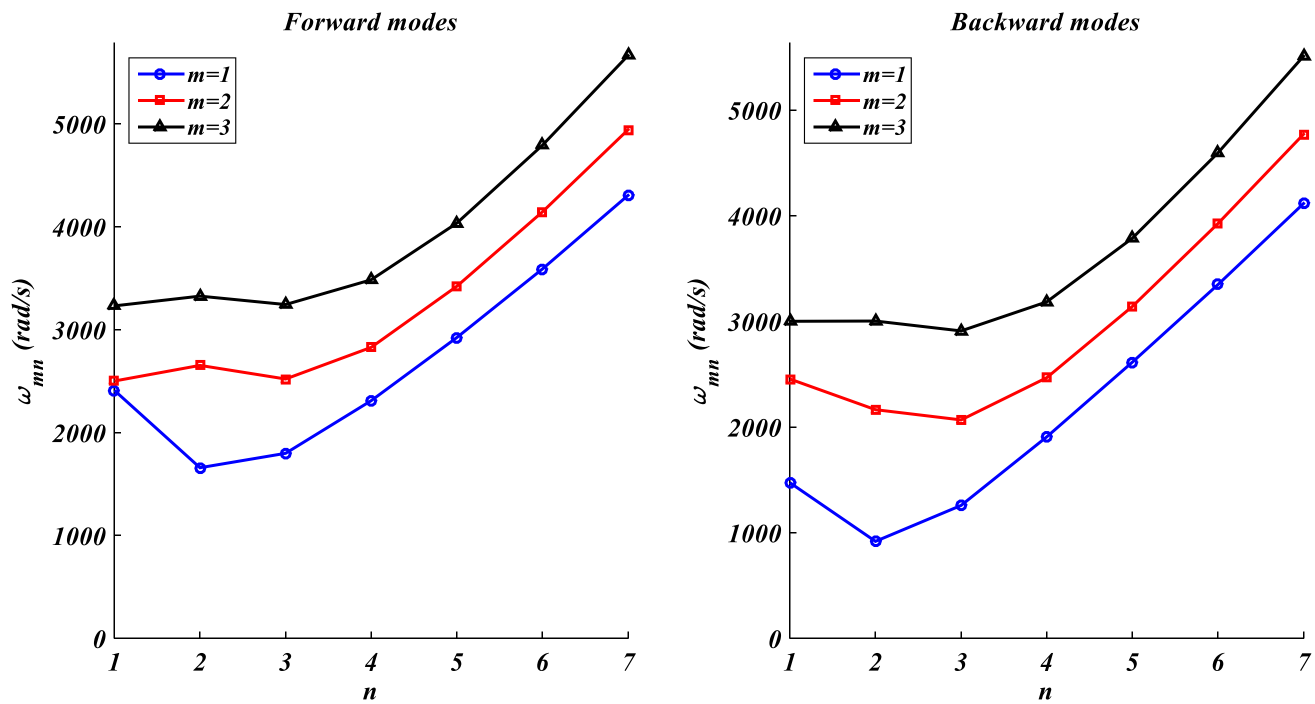

Fig. 3 Effect of circumferential mode number on the forward and backward frequencies of the shell

Table 4 Effect of boundary conditions on the forward and backward frequencies of the shell

n		*m*	CC	SC	CS	SS	FC	CF
1	Forward	1	2474.444	2420.392	2410.094	2207.664	1915.779	917.8133
		2	3262.936	3210.424	2500.862	2418.169	2928.790	2341.068
		3	3761.422	3737.353	3231.327	3090.926	3238.553	2910.980
	Backward	1	1599.276	1564.826	1473.369	1465.050	935.1589	59.78743
		2	2851.743	2827.447	2454.527	2214.097	2276.995	1822.798
		3	3511.507	3498.870	3000.722	2786.025	3043.634	2849.230
2	Forward	1	1820.777	1753.604	1658.450	1594.344	1364.714	1050.558
		2	2758.933	2714.134	2652.927	2622.019	2140.192	1858.789
		3	3481.664	3443.141	3326.099	3287.006	3028.432	2886.449
	Backward	1	1135.714	1065.243	918.0316	854.1163	615.9952	364.7010
		2	2226.313	2176.896	2164.396	2120.007	1503.413	1232.697
		3	3143.231	3097.222	3003.189	2960.282	2588.657	2485.024
3	Forward	1	1909.564	1872.494	1798.372	1765.576	1808.503	1550.555
		2	2584.914	2525.451	2520.593	2463.807	2183.048	1925.112
		3	3376.556	3310.173	3244.139	3184.233	2865.448	2746.053
	Backward	1	1399.870	1359.201	1258.020	1223.945	1286.103	1042.480
		2	2134.948	2069.667	2067.379	2001.382	1683.038	1431.164
		3	3029.421	2954.754	2909.665	2841.653	2445.666	2341.949
4	Forward	1	2387.900	2381.245	2309.981	2305.331	2379.426	2098.918
		2	2897.215	2864.189	2828.221	2798.954	2802.516	2414.927
		3	3604.141	3543.182	3484.840	3430.720	3279.343	3015.033
	Backward	1	2005.311	1997.974	1906.692	1901.937	1996.187	1717.234
		2	2540.410	2503.868	2466.619	2433.423	2435.741	2033.685
		3	3299.112	3231.758	3184.319	3123.399	2936.820	2677.797

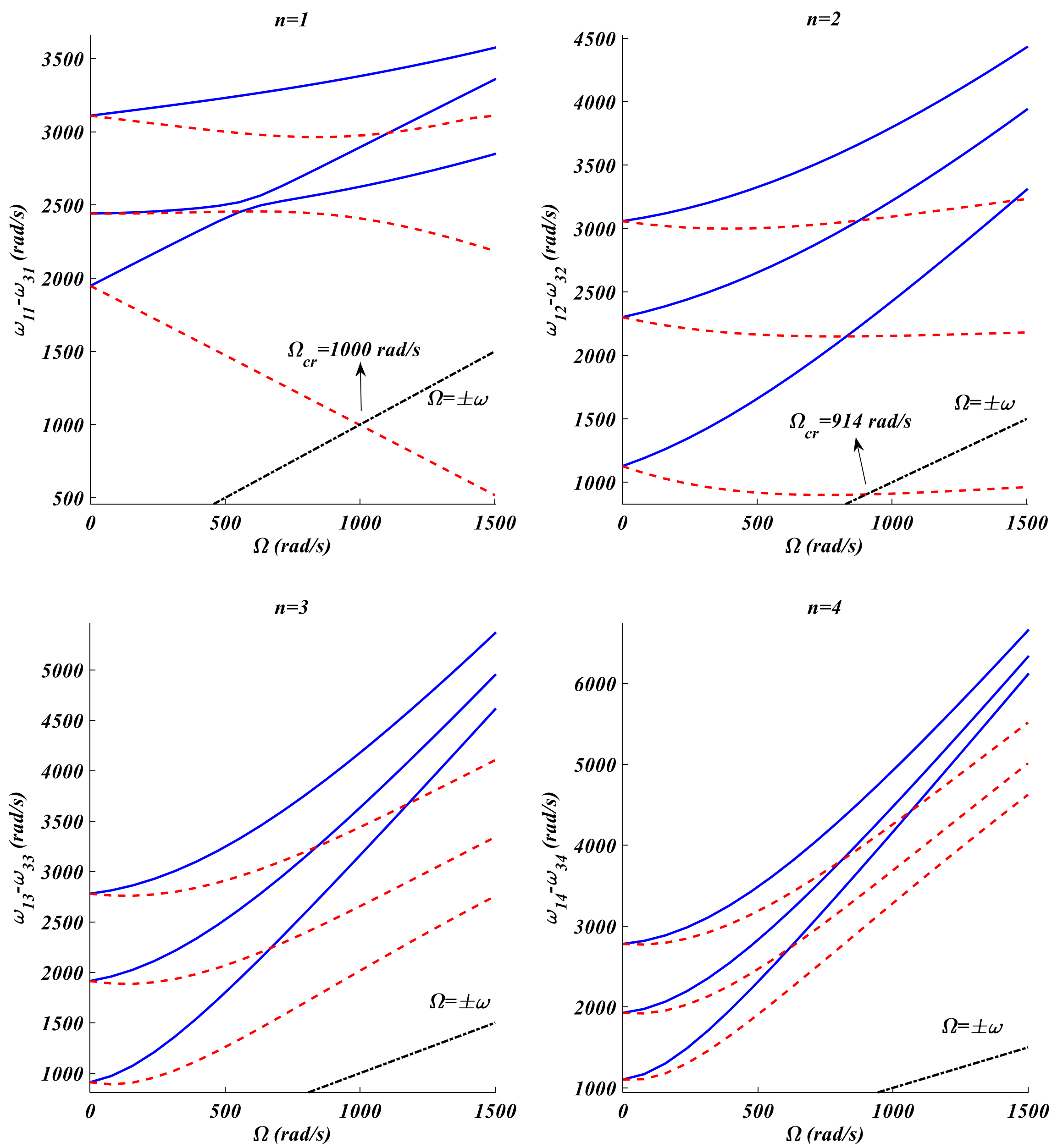

Fig. 4 Effect of angular velocity on the forward (-) and backward (–) frequencies of the shell

$l_{\mathrm{GNP}}=0.5$ and $h_{\mathrm{GNP}}/l_{\mathrm{GNP}}=0.5\times10^{-3}$. Also it should be noted that the natural frequencies are denoted by ω_{mn} in which "n" indicates to circumferential mode number [Eq. (33)] and $m=1,2,3,\ldots$ shows the sequence of modes in meridional direction (x-axis).

Table 1 shows the effect of the number of grid points [N in Eq. (36)] on the values of forward and backward frequencies of the shell. As shown in this table, the presented solution converges rapidly and what follows, all of the numerical examples are reported based on $N=13$.

In order to confirm the accuracy of the presented solution, consider a CC stationary homogenous truncated conical shell of $\nu=0.3$, $\alpha=45°$, $h/b=0.01$ and $L\sin\alpha/b=0.5$. For various values of circumferential mode number, values of dimensionless natural frequency ($\omega^{*}=\omega b[\rho(1-\nu^{2})/E]^{0.5}$) are presented in Table 2 for $m=1$ against corresponding

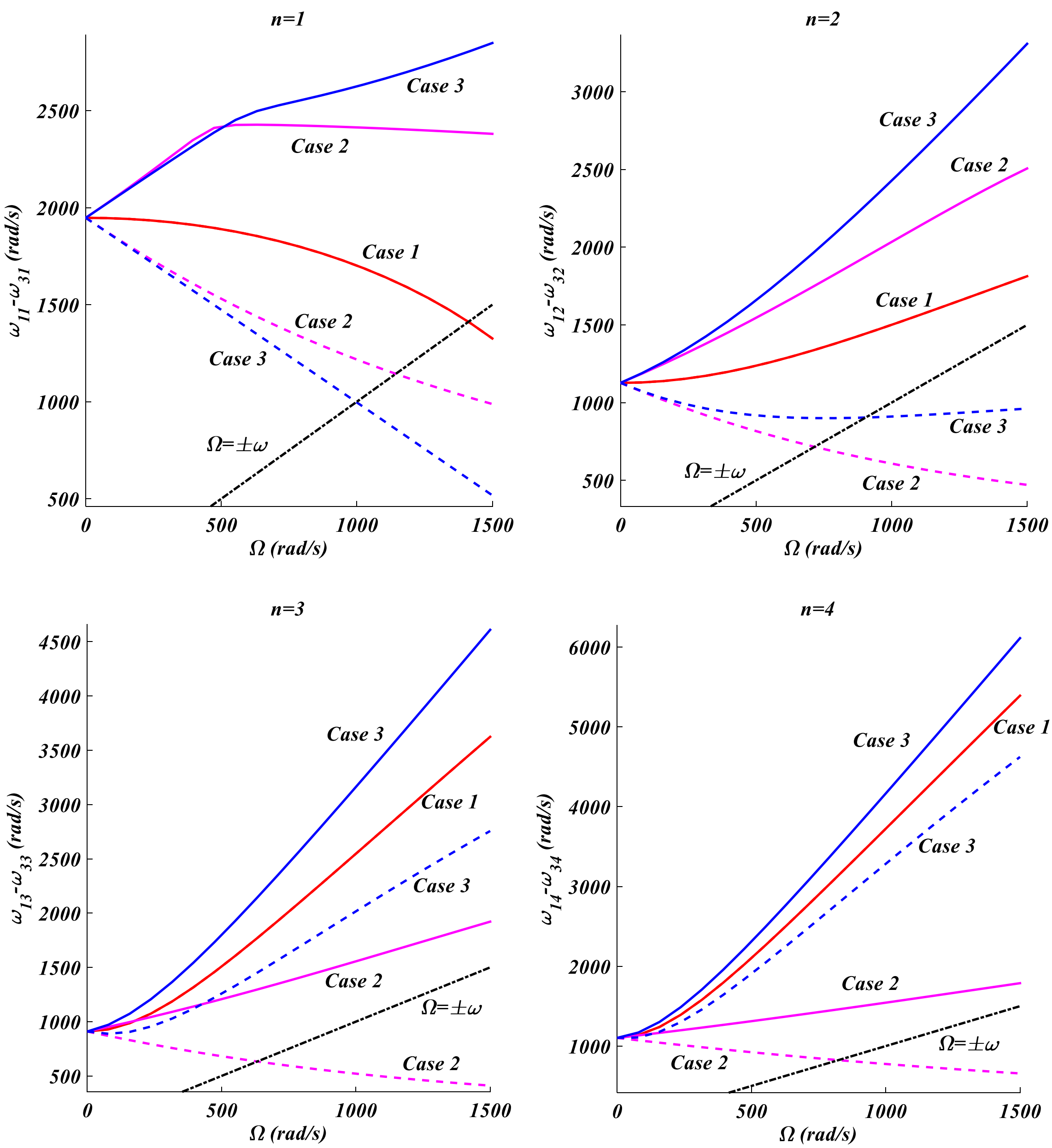

Fig. 5 Effect of centrifugal and Coriolis accelerations and initial hoop tension on the forward (-) and backward (–) frequencies of the shell

ones reported by Liew et al. [36] and Shu [37]. This table confirms that the presented solution has high accuracy and results are in agreement with those reported by other authors. It is worth mentioning that in Refs. [36, 37] the shear deformation and rotational inertia are neglected and the natural frequencies are obtained higher than the more accurate ones predicted in the presented paper based on the FSDT.

An homogenous rotating truncated conical shell of $\alpha = 30°$, $L/a = 6$, $h/a = 0.01$ and $\nu = 0.3$ is considered. For different boundary conditions, two selected values of dimensionless angular velocity ($\Omega^* = \Omega b[\rho(1-\nu^2)/E]^{0.5}$) and $n = m = 1$, dimensionless values of the forward and backward frequencies ($\omega^* = \omega b[\rho(1-\nu^2)/E]^{0.5}$) are presented in Table 3 against corresponding ones reported by Dai et al. [32]. This table confirms that values of the frequencies are in high agreement and results with high accuracy can be obtained using the presented numerical solution. It should be noted that Dai et al. [32] used a classical shell theory to model the shell, and values of the both forward and

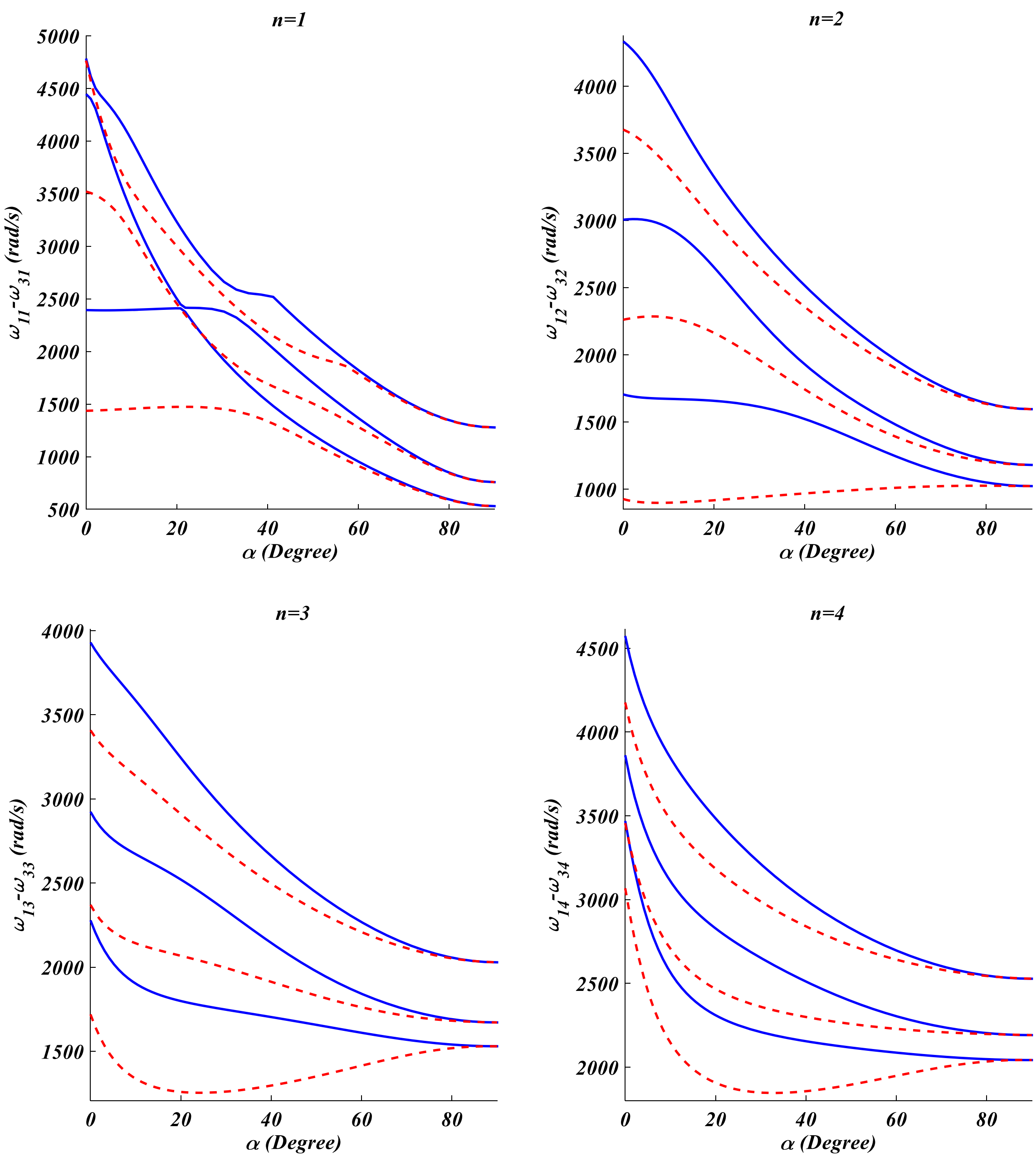

Fig. 6 Effect of semi-vertex angle on the forward (-) and backward (--) frequencies

backward frequencies reported by them are higher than the more accurate ones achieved in the presented paper. Also it is worth mentioning that the definition of forward and backward frequencies in Ref. [32] is reverse of the definition used in the current papers.

Effect of circumferential mode number on the values of forward and backward frequencies of the rotating GNP-reinforced truncated conical shells is illustrated in Fig. 3. This figure shows that for a special value of circumferential mode number, the minimum values of forward and backward frequencies can be obtained. Figure 3 reveals that this special value of circumferential mode number is same for forward and backward frequencies but is not same for different meridional mode numbers.

Effect of boundary conditions on the forward and backward frequencies of the rotating GNP-reinforced truncated

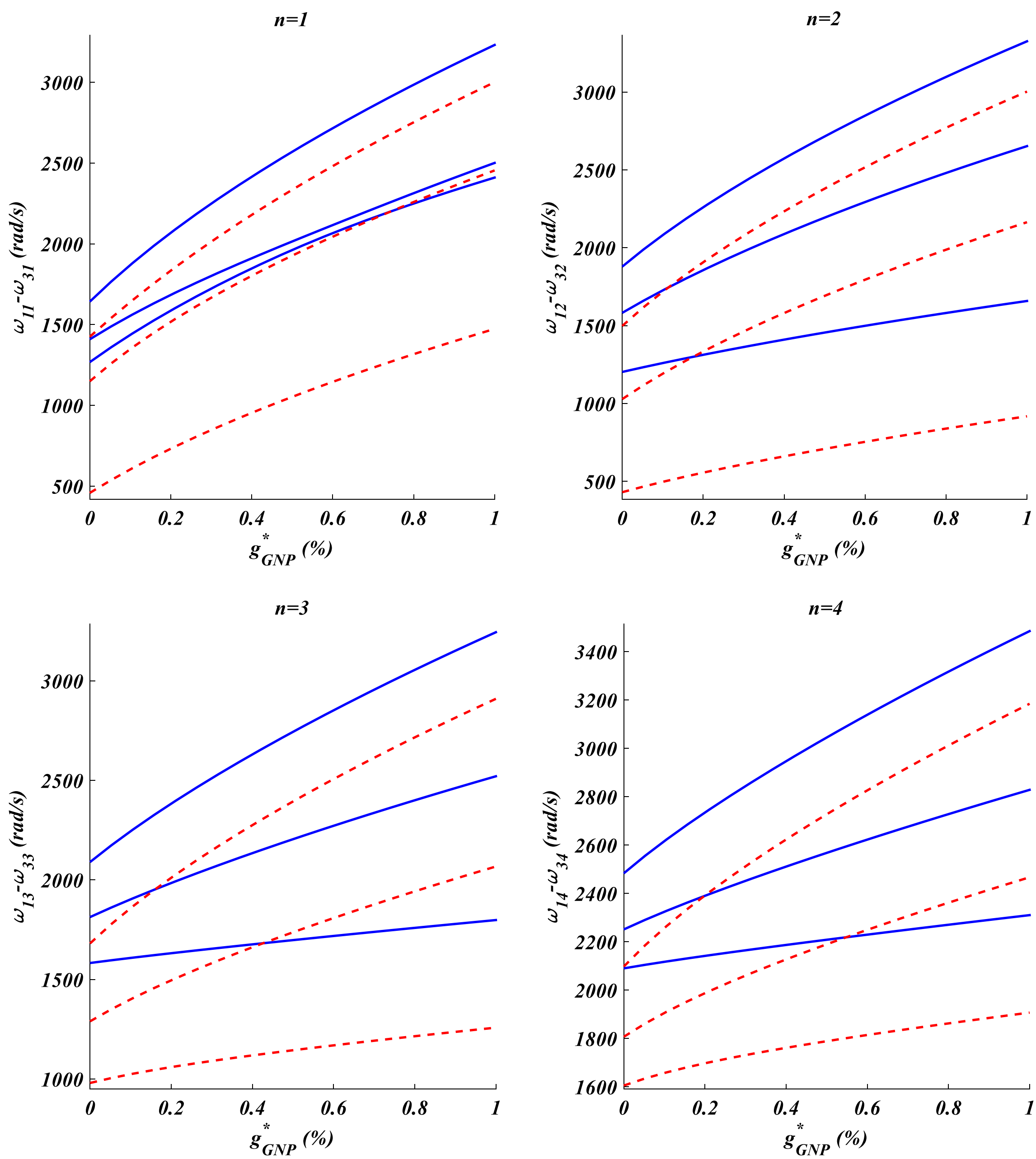

Fig. 7 Effect of total mass fraction of GNPs on the forward (-) and backward (–) frequencies

conical shells is investigated in Table 4. This table shows that as was expected, using more constrained conditions at the edges of the shell leads to increase in values of forward and backward frequencies. A simple comparison between results for SC and CS or FC and CF shells reveals that in order to increase values of forward and backward frequencies it is better to use more constrained conditions at $x = L$ (large radius of the cone) rather that $x = 0$ (small radius of the cone). It is noteworthy that result of this table can be used as benchmark results for other researchers.

As rotational speed of the shell rises, both the Coriolis acceleration and initial hoop tension increase. The initial hoop tension leads to increase in stiffness of the shell and increases both forward and backward frequencies, but the Coriolis acceleration increases forward frequencies and reduces backward ones. Figure 4 shows the influence

Table 5 Effect of distribution pattern of GNPs on the forward and backward frequencies

n		m	FG-O	FG-V	FG-A	UD	FG-X
1	Forward	1	2411.381	2419.388	2410.094	2417.615	2422.468
		2	2488.552	2490.278	2500.862	2501.856	2512.996
		3	3198.122	3224.119	3231.327	3255.517	3299.813
	Backward	1	1471.346	1473.823	1473.369	1475.529	1479.520
		2	2437.108	2441.553	2454.527	2458.276	2475.724
		3	2980.749	2981.036	3000.722	3000.859	3019.469
2	Forward	1	1647.360	1658.119	1658.450	1669.334	1689.570
		2	2626.990	2650.808	2652.927	2678.233	2726.588
		3	3249.840	3322.254	3326.099	3400.493	3534.883
	Backward	1	894.3988	892.7373	918.0316	916.0112	935.9404
		2	2121.864	2127.729	2164.396	2170.989	2217.660
		3	2913.432	2958.538	3003.189	3050.508	3175.981
3	Forward	1	1768.808	1798.270	1798.372	1828.177	1882.633
		2	2466.202	2520.099	2520.593	2576.291	2678.385
		3	3141.628	3243.006	3244.139	3349.344	3539.218
	Backward	1	1200.548	1202.228	1258.020	1259.018	1312.640
		2	1979.876	2003.288	2067.379	2090.905	2192.931
		3	2775.612	2840.641	2909.665	2977.035	3161.491
4	Forward	1	2257.177	2309.843	2309.981	2363.077	2459.682
		2	2728.989	2827.724	2828.221	2928.106	3107.537
		3	3329.011	3483.922	3484.840	3642.514	3922.327
	Backward	1	1812.215	1823.374	1906.692	1916.799	2012.102
		2	2319.082	2372.316	2466.619	2518.642	2697.351
		3	2980.623	3086.384	3184.319	3290.389	3566.159

of rotational speed on the natural frequencies of the shell which is known as the Campbell diagram [27]. As depicted in this figure, with increase in rotational speed of the shell, all forward frequencies grow which shows the cooperative effects of initial hoop tension and the Coriolis acceleration on the forward modes. Figure 4 shows different trends for backward modes; for $n=1$ and $n=2$, with increase in rotational speed, some backward frequencies decrease, some of them increase and other ones decrease at first and increase subsequently, and for $n\geq 3$, all backward frequencies grow with increase in rotational speed of the shell. This different trends can be explained by the contrast between effects of initial hoop tension and the Coriolis acceleration on the backward modes.

In Fig. 4, the line of $\Omega = \pm\omega$ is shown as well which is known as the line of synchronous whirling [27]. Intersection of this line with the Campbell diagram determines the critical resonance speeds of the rotating shell which should be strongly avoided. At these critical speeds, any residual unbalance increases the amplitude of vibration and leads to a catastrophic failure. As shown in this figure for the current case study, the resonance speeds can be found for $n=1$ ($\Omega_{cr}\approx 1000$ rad/s) and $n=2$ ($\Omega_{cr}\approx 914$ rad/s), and for higher values of the circumferential mode number ($n\geq 3$) the line of synchronous whirling has no intersection with the Campbell diagram and no resonance speed can be found.

In order to investigated the influences of centrifugal and Coriolis accelerations and initial hoop tension, variation of forward and backward frequencies is depicted in Fig. 5 versus rotational speed for $m=1$, and three cases which are determined based on Eq. (31) as follows:

Case 1 Centrifugal acceleration and initial hoop tension (terms contain square of rotational speed) are considered but Coriolis acceleration (terms contain rotational speed and first time derivatives of displacements) is neglected.
Case 2 Coriolis acceleration is considered but centrifugal acceleration and initial hoop tension are neglected.
Case 3 Coriolis and centrifugal accelerations and initial hoop tension are considered.

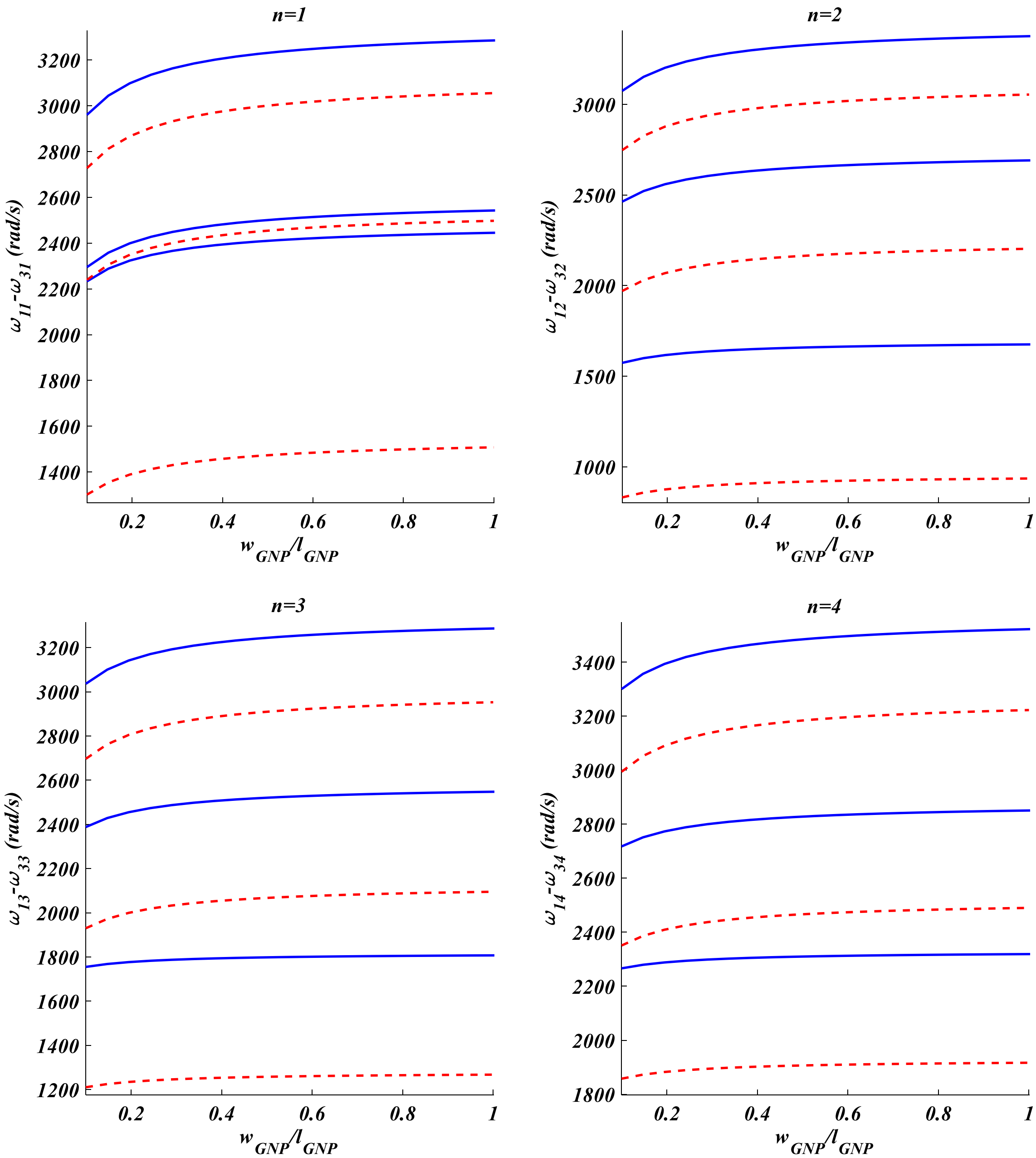

Fig. 8 Effect of width of the GNPs on the forward (-) and backward (–) frequencies

As depicted in Fig. 5, for a stationary shell there is no difference between three cases, but as rotating speed of the shell increases, significant differences can be seen between all cases. This figure shows that by neglecting Coriolis acceleration (Case 1) no difference can be detected between forward and backward frequencies and values of the natural frequencies are between corresponding values of forward and backward frequencies predicted in Case 3. Figure 5 reveals that centrifugal acceleration and initial hoop tension play predominant roles in determining values of critical speeds of the rotating shells. A comparison between cases 2 and 3 in this figure that reveals that for $n=1{,}2$ neglecting centrifugal acceleration and initial hoop tension generates error in prediction of values of the critical speed, and for $n>2$ the critical speeds predicted in case 2 vanish as the

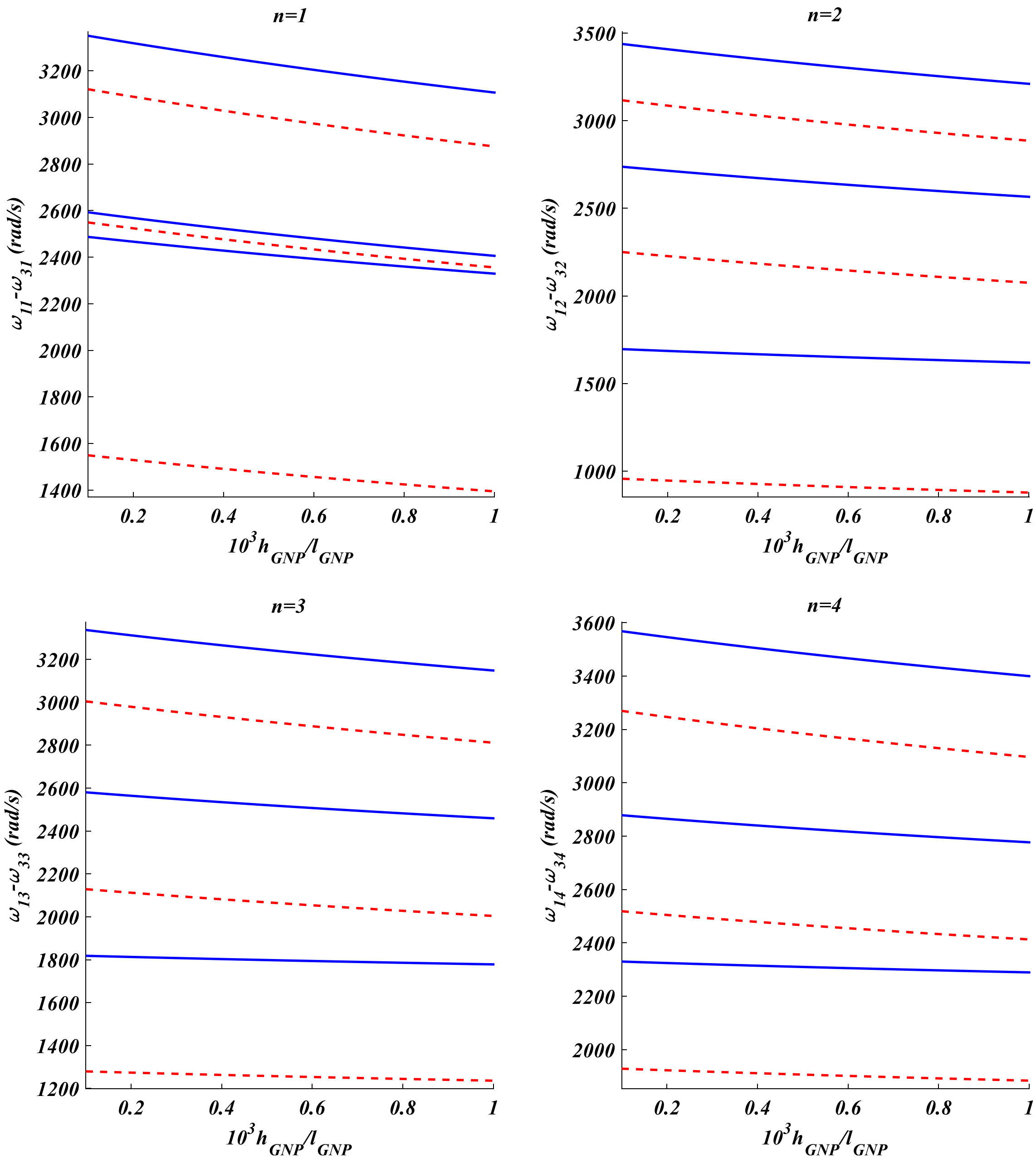

Fig. 9 Effect of thickness of the GNPs on the forward (-) and backward (–) frequencies

centrifugal acceleration and initial hoop tension are considered (case 3).

Figure 6 shows the influence of the semi-vertex angle on the forward and backward frequencies of the shell. As depicted in this figure, increase in value of the semi-vertex angle from $\alpha = 0$ (cylindrical shell of radius $r = a$) to $\alpha = 90°$ (circular annular plate of inner radius $r = a$ and outer radius $r = b$) leads to reduction in forward frequencies but no specific trend can be seen for backward ones, and these modes may increase or decrease with increase in value of semi-vertex angle. For explain this, it should be noted that with specific values of small radius and length of the shell, increase in value of semi-vertex angle of the shell affects both stiffness and inertia of the shell.

Figure 6 also shows that for high values of semi-vertex angle forward and backward frequencies reach to same values which are corresponding natural frequencies of a rotating annular circular plate of inner radius $r = a$ and outer radius $r = b$.

Figure 7 shows the influence of total mass fraction of GNPs on the forward and backward frequencies of the rotating GNP-reinforced truncated conical shells for different values of circumferential mode number. As shown in this figure, subjoining a small amount of GNPs to the epoxy leads to a significant increase in the values of the forward and backward frequencies. It can be explained by high value of the modulus of elasticity of the GNPs which is significantly greater than modulus of elasticity of the epoxy.

Table 5 shows values of the forward and backward frequencies of the rotating GNP-reinforced truncated conical shell for different types of GNPs distribution patterns. This table reveals that among all studied patterns, the highest values of the forward and backward frequencies belong to FG-X pattern and the lowest ones belong to FG-O pattern. In other words, in order to make the most increase in the values of the forward and backward frequencies, it is better to put the GNPs as far as away from the middle surface of the shell which creates the highest flexural stiffness.

Variation of forward and backward frequencies of the GNP-reinforced truncated conical shells versus width of the GNPs is depicted in Fig. 8. As shown in this figure, increase in the width of the GNPs slightly increases both forward and backward frequencies of GNP-reinforced conical shells. In other words, increase in surface area of the GNPs increases the stiffness of a GNP-reinforced structure. To explain this, it can be pointed that a larger contact area between the GNPs and the polymer matrix provides better load transfer capability.

Figure 9 shows the influence of thickness of the GNPs on forward and backward frequencies of the GNP-reinforced truncated conical shells. This figure shows that increase in thickness of the GNPs leads to a slight reduction in both forward and backward frequencies which can be explained by increase in the monolayer graphene sheets. Figures 8 and 9 confirm that in order to have a better reinforcing effect, GNPs with larger surface area and fewer monolayer graphene sheets should be used.

5 Conclusions

Using GDQM, a numerical solution was presented for free vibration analysis of rotating truncated conical shells made of GNP-reinforced epoxy. The shell was modeled based on the FSDT incorporating centrifugal and Coriolis accelerations and initial hoop tension. Numerical results confirmed that presented solution is convergent, and for a special value of the circumferential mode number, the minimum values can be achieved for both forward and backward frequencies. It was shown that centrifugal and coriolis accelerations and initial hoop tension play predominant roles in dynamics of rotating conical shells. It was concluded that as rotational speed of the shell increases, forward frequencies increase, but no specific trend can be stated for variation of backward frequencies versus variation of rotational speed. Numerical results confirmed that increase in values of the semi-vertex angle decreases forward frequencies, but no specific trend can be stated for the effect of semi-vertex angle on the variation of backward frequencies. It was shown by numerical examples that increase in the value of the mass fraction of GNPs significantly increases values of both forward and backward frequencies, and in order to achieve higher reinforcing effect, it is better to use the GNPs with a larger surface area and fewer monolayer graphene and put them as far as away from the middle surface of the shell.

Appendix A

In Eq. (41) mass, gyroscopic and stiffness matrices and displacement vector are defined as follows:

$$\{s\}_{5N\times1} = \begin{Bmatrix} \{U\} \\ \{V\} \\ \{W\} \\ \{X\} \\ \{\Theta\} \end{Bmatrix}, \quad [M] = \begin{bmatrix} m_{11} & [0] & [0] & m_{14} & [0] \\ [0] & m_{22} & [0] & [0] & m_{25} \\ [0] & [0] & m_{33} & [0] & [0] \\ m_{41} & [0] & [0] & m_{44} & [0] \\ [0] & m_{52} & [0] & [0] & m_{55} \end{bmatrix},$$
$$[G] = \begin{bmatrix} [0] & g_{12} & [0] & [0] & g_{15} \\ g_{21} & [0] & g_{23} & g_{24} & [0] \\ [0] & g_{32} & [0] & [0] & g_{35} \\ [0] & g_{42} & [0] & [0] & g_{45} \\ g_{51} & [0] & g_{53} & g_{54} & [0] \end{bmatrix}, \quad [K] = \begin{bmatrix} k_{11} & k_{12} & k_{13} & k_{14} & k_{15} \\ k_{21} & k_{22} & k_{23} & k_{24} & k_{25} \\ k_{31} & k_{32} & k_{33} & k_{34} & k_{35} \\ k_{41} & k_{42} & k_{43} & k_{44} & k_{45} \\ k_{51} & k_{52} & k_{53} & k_{54} & k_{55} \end{bmatrix}, \tag{A-1}$$

in which **[0]** is zero matrix of order N and

$$
\begin{aligned}
&k_{11} = A_{11}[B] + A_{11}\sin\alpha\left[a_1\right][A] - \left(A_{22}\sin^2\alpha + A_{66}n^2\right)\left[a_2\right] - n^2 I_0\Omega^2 I,\\
&k_{12} = n\left(A_{12} + A_{66}\right)\left[a_1\right][A] - n\left(A_{22} + A_{66}\right)\sin\alpha\left[a_2\right] - 2nI_0\Omega^2\sin\alpha I,\\
&k_{13} = A_{12}\cos\alpha\left[a_1\right][A] - 0.5\sin 2\alpha A_{22}\left[a_2\right],\\
&k_{14} = B_{11}[B] + B_{11}\sin\alpha\left[a_1\right][A] - \left(B_{22}\sin^2\alpha + B_{66}n^2\right)\left[a_2\right] - n^2 I_1\Omega^2 I,\\
&k_{15} = n\left(B_{12} + B_{66}\right)\left[a_1\right][A] - n\left(B_{22} + B_{66}\right)\sin\alpha\left[a_2\right] - 2nI_1\Omega^2\sin\alpha I,\\
&g_{12} = 2\Omega I_0\sin\alpha I,\ g_{15} = 2\Omega I_1\sin\alpha I,\\
&m_{11} = I_0 I,\ m_{14} = I_1 I,\\
&k_{21} = -n\left(A_{12} + A_{66}\right)\left[a_1\right][A] - n\left(A_{22} + A_{66}\right)\sin\alpha\left[a_2\right] - 2nI_0\Omega^2\sin\alpha I,\\
&k_{22} = A_{66}[B] + A_{66}\sin\alpha\left[a_1\right][A] - \left(A_{22}n^2 + A_{44}\cos^2\alpha + A_{66}\sin^2\alpha\right)\left[a_2\right] - n^2 I_0\Omega^2 I,\\
&k_{23} = -n\left(A_{22} + A_{44}\right)\cos\alpha\left[a_2\right] - 2nI_0\Omega^2\cos\alpha I,\\
&k_{24} = -n\left(B_{12} + B_{66}\right)\left[a_1\right][A] - n\left(B_{22} + B_{66}\right)\sin\alpha\left[a_2\right] - 2nI_1\Omega^2\sin\alpha I,\\
&k_{25} = B_{66}[B] + B_{66}\sin\alpha\left[a_1\right][A] + A_{44}\cos\alpha\left[a_1\right] - \left(B_{22}n^2 + B_{66}\sin^2\alpha\right)\left[a_2\right] - n^2 I_1\Omega^2 I,\\
&g_{21} = 2I_0\Omega\sin\alpha I,\ g_{23} = 2I_0\Omega\cos\alpha I,\ g_{24} = 2I_1\Omega\sin\alpha I,\\
&m_{22} = I_0 I,\ m_{25} = I_1 I,\\
&k_{31} = -A_{12}\cos\alpha\left[a_1\right][A] - 0.5\sin 2\alpha A_{22}\left[a_2\right],\\
&k_{32} = -n\left(A_{22} + A_{44}\right)\cos\alpha\left[a_2\right] - 2nI_0\Omega^2\cos\alpha I,\\
&k_{33} = A_{55}[B] + A_{55}\sin\alpha\left[a_1\right][A] - \left(A_{22}\cos^2\alpha + A_{44}n^2\right)\left[a_2\right] - n^2 I_0\Omega^2 I,\\
&k_{34} = \left(A_{55}I - B_{12}\cos\alpha\left[a_1\right]\right)[A] + A_{55}\sin\alpha\left[a_1\right] - 0.5B_{22}\sin 2\alpha\left[a_2\right],\\
&k_{35} = n\left(A_{44}\left[a_1\right] - B_{22}\cos\alpha\left[a_2\right]\right) - 2nI_1\Omega^2\cos\alpha I,\\
&g_{32} = 2I_0\Omega\cos\alpha I,\ g_{35} = 2I_1\Omega\cos\alpha I,\\
&m_{33} = I_0 I,\\
&k_{41} = B_{11}[B] + B_{11}\sin\alpha\left[a_1\right][A] - \left(B_{22}\sin^2\alpha + B_{66}n^2\right)\left[a_2\right] - n^2 I_1\Omega^2 I,\\
&k_{42} = n\left(B_{12} + B_{66}\right)\left[a_1\right][A] - n\left(B_{22} + B_{66}\right)\sin\alpha\left[a_2\right] - 2nI_1\Omega^2\sin\alpha I,\\
&k_{43} = -A_{55}[A] + B_{12}\cos\alpha\left[a_1\right][A] - 0.5\sin 2\alpha B_{22}\left[a_2\right],\\
&k_{44} = D_{11}[B] + D_{11}\sin\alpha\left[a_1\right][A] - \left(D_{22}\sin^2\alpha + D_{66}n^2\right)\left[a_2\right] - \left(A_{55} + n^2 I_2\Omega^2\right)I,\\
&k_{45} = n\left(D_{12} + D_{66}\right)\left[a_1\right][A] - n\left(D_{22} + D_{66}\right)\sin\alpha\left[a_2\right] - 2nI_2\Omega^2\sin\alpha I,\\
&g_{42} = 2I_1\Omega\sin\alpha I,\ g_{45} = 2I_2\Omega\sin\alpha I,\\
&m_{41} = I_1 I,\ m_{44} = I_2 I,\\
&k_{51} = -n\left(B_{12} + B_{66}\right)\left[a_1\right][A] - n\left(B_{22} + B_{66}\right)\sin\alpha\left[a_2\right] - 2nI_1\Omega^2\sin\alpha I,\\
&k_{52} = B_{66}[B] + B_{66}\sin\alpha\left[a_1\right][A] + A_{44}\cos\alpha\left[a_1\right] - \left(B_{22}n^2 + B_{66}\sin^2\alpha\right)\left[a_2\right] - n^2 I_1\Omega^2 I,\\
&k_{53} = n\left(A_{44}\left[a_1\right] - B_{22}\cos\alpha\left[a_2\right]\right) - 2nI_1\Omega^2\cos\alpha I,\\
&k_{54} = -n\left(D_{12} + D_{66}\right)\left[a_1\right][A] - n\left(D_{22} + D_{66}\right)\sin\alpha\left[a_2\right] - 2nI_2\Omega^2\sin\alpha I,\\
&k_{55} = D_{66}[B] + D_{66}\sin\alpha\left[a_1\right][A] - \left(D_{22}n^2 + D_{66}\sin^2\alpha\right)\left[a_2\right] - \left(A_{44} + n^2 I_2\Omega^2\right)I,\\
&g_{51} = 2I_1\Omega\sin\alpha I,\ g_{53} = 2I_1\Omega\cos\alpha I,\ g_{54} = 2I_2\Omega\sin\alpha I,\\
&m_{52} = I_1 I,\ m_{55} = I_2 I,
\end{aligned} \tag{A-2}
$$

where **I** is identity matrix of order N and $[\mathbf{a_1}]$ and $[\mathbf{a_2}]$ are two diagonal matrices defined as follows:

$$\left[a_1\right]_{ii} = \frac{1}{r_i},\ \left[a_2\right]_{ii} = \frac{1}{r_i^2}. \tag{A-3}$$

Appendix B

In Eq. (42), matrix $[\mathbf{T}]$ is defined as

$$[T]_{10\times 5N} = \begin{bmatrix} T_{11} & T_{12} & T_{13} & T_{14} & T_{15} \\ T_{21} & T_{22} & T_{23} & T_{24} & T_{25} \\ \vdots & \vdots & \vdots & \vdots & \vdots \\ T_{101} & T_{102} & T_{103} & T_{104} & T_{105} \end{bmatrix}, \tag{B-1}$$

in which $\mathbf{T_{11}} - \mathbf{T_{55}}$ are associated with the conditions at $x=0$ and are defined as follows:

$$\begin{aligned}
&\text{Clamped}\,(C):\\
&T_{11} = T_{22} = T_{33} = T_{44} = T_{55} = I_1,\\
&T_{12} = T_{13} = T_{14} = T_{15} = T_{21} = T_{23} = T_{24} = T_{25} = T_{31} = T_{32} = T_{34} =\\
&T_{35} = T_{41} = T_{42} = T_{43} = T_{45} = T_{51} = T_{52} = T_{53} = T_{54} = \{0\}_{1\times N},\\
&\text{Simply Supported}\,(S):\\
&T_{11} = A_{11}A_1 + \frac{A_{12}\sin\alpha}{a}I_1, T_{14} = T_{41} = B_{11}A_1 + \frac{B_{12}\sin\alpha}{a}I_1,\\
&T_{44} = D_{11}A_1 + \frac{D_{12}\sin\alpha}{a}I_1, T_{22} = T_{33} = T_{55} = I_1,\\
&T_{12} = T_{13} = T_{15} = T_{21} = T_{23} = T_{24} = T_{25} = T_{31} = T_{32} = T_{34} =\\
&T_{35} = T_{42} = T_{43} = T_{45} = T_{51} = T_{52} = T_{53} = T_{54} = \{0\}_{1\times N},\\
&\text{Free}\,(F):\\
&T_{11} = A_{11}A_1 + \frac{A_{12}\sin\alpha}{a}I_1, T_{12} = \frac{nA_{12}}{a}I_1, T_{13} = \frac{A_{12}\cos\alpha}{a}I_1,\\
&T_{14} = B_{11}A_1 + \frac{B_{12}\sin\alpha}{a}I_1, T_{15} = \frac{nB_{12}}{a}I_1,\\
&T_{21} = -\frac{nA_{66}}{a}I_1, T_{22} = A_{66}A_1 - \frac{A_{66}\sin\alpha}{a}I_1, T_{23} = \{0\}_{1\times N},\\
&T_{24} = -\frac{nB_{66}}{a}I_1, T_{25} = B_{66}A_1 - \frac{B_{66}\sin\alpha}{a}I_1,\\
&T_{31} = T_{32} = T_{35} = \{0\}_{1\times N}, T_{33} = A_1, T_{34} = I_1,\\
&T_{41} = B_{11}A_1 + \frac{B_{12}\sin\alpha}{a}I_1, T_{42} = \frac{nB_{12}}{a}I_1,\\
&T_{43} = \frac{B_{12}\cos\alpha}{a}I_1, T_{44} = D_{11}A_1 + \frac{D_{12}\sin\alpha}{a}I_1,\\
&T_{45} = \frac{nD_{12}}{a}I_1, T_{51} = -\frac{nB_{66}}{a}I_1, T_{52} = B_{66}A_1 - \frac{B_{66}\sin\alpha}{a}I_1,\\
&T_{53} = \{0\}_{1\times N}, T_{54} = -\frac{D_{66}n}{a}I_1, T_{55} = D_{66}A_1 - \frac{D_{66}\sin\alpha}{a}I_1,
\end{aligned} \tag{B-2}$$

in which the subscript 1 indicates to the first row of each matrix.

Also, with the following definitions, $\mathbf{T_{61}} - \mathbf{T_{105}}$ are associated with the conditions at $x=L$:

$$\begin{aligned}
&\text{Clamped}\,(C):\\
&T_{61} = T_{72} = T_{83} = T_{94} = T_{105} = I_N,\\
&T_{62} = T_{63} = T_{64} = T_{65} = T_{71} = T_{73} = T_{74} = T_{75} = T_{81} = T_{82} = T_{84} =\\
&T_{85} = T_{91} = T_{92} = T_{93} = T_{95} = T_{101} = T_{102} = T_{103} = T_{104} = \{0\}_{1\times N},\\
&\text{Simply Supported}\,(S):\\
&T_{61} = A_{11}A_N + \frac{A_{12}\sin\alpha}{b}I_N, T_{64} = T_{91} = B_{11}A_N + \frac{B_{12}\sin\alpha}{b}I_N,\\
&T_{94} = D_{11}A_N + \frac{D_{12}\sin\alpha}{b}I_N, T_{72} = T_{83} = T_{105} = I_N,\\
&T_{62} = T_{63} = T_{65} = T_{71} = T_{73} = T_{74} = T_{75} = T_{81} = T_{82} = T_{84} =\\
&T_{85} = T_{92} = T_{93} = T_{95} = T_{101} = T_{102} = T_{103} = T_{104} = \{0\}_{1\times N},\\
&\text{Free}\,(F):\\
&T_{61} = A_{11}A_N + \frac{A_{12}\sin\alpha}{b}I_N, T_{62} = \frac{nA_{12}}{b}I_N, T_{63} = \frac{A_{12}\cos\alpha}{b}I_N,\\
&T_{64} = B_{11}A_N + \frac{B_{12}\sin\alpha}{b}I_N, T_{65} = \frac{nB_{12}}{b}I_N, T_{71} = -\frac{nA_{66}}{b}I_N,\\
&T_{72} = A_{66}A_N - \frac{A_{66}\sin\alpha}{b}I_N, T_{73} = \{0\}_{1\times N}, T_{74} = -\frac{nB_{66}}{b}I_N,\\
&T_{75} = B_{66}A_N - \frac{B_{66}\sin\alpha}{b}I_N, T_{81} = T_{82} = T_{85} = \{0\}_{1\times N},\\
&T_{83} = A_N, T_{84} = I_N, T_{91} = B_{11}A_N + \frac{B_{12}\sin\alpha}{b}I_N, T_{92} = \frac{nB_{12}}{b}I_N,\\
&T_{93} = \frac{B_{12}\cos\alpha}{b}I_N, T_{94} = D_{11}A_N + \frac{D_{12}\sin\alpha}{b}I_N, T_{95} = \frac{nD_{12}}{b}I_N,\\
&T_{101} = -\frac{nB_{66}}{b}I_N, T_{102} = B_{66}A_N - \frac{B_{66}\sin\alpha}{b}I_N, T_{103} = \{0\}_{1\times N},\\
&T_{104} = -\frac{D_{66}n}{b}I_N, T_{105} = D_{66}A_N - \frac{D_{66}\sin\alpha}{b}I_N,
\end{aligned} \tag{B-3}$$

in which the subscript N indicates to the last row of each matrix.

References

1. Habibi M, Mohammadgholiha M, Safarpour H (2019) Wave propagation characteristics of the electrically GNP-reinforced nanocomposite cylindrical shell. J Braz Soc Mech Sci Eng 41:221
2. Barati MR, Shahverdi H (2020) Finite element forced vibration analysis of refined shear deformable nanocomposite graphene platelet-reinforced beams. J Braz Soc Mech Sci Eng 42:33
3. Zhao S, Yang Z, Kitipornchai S, Yang J (2020) Dynamic instability of functionally graded porous arches reinforced by graphene platelets. Thin-Walled Struct 147:106491
4. Afshari H, Adab N (2020) Size-dependent buckling and vibration analyses of GNP reinforced microplates based on the quasi-3D sinusoidal shear deformation theory. Mech Based Des Struct Mach. https://doi.org/10.1080/15397734.2020.1713158
5. Nguyen NV, Nguyen-Xuan H, Lee D, Lee J (2020) A novel computational approach to functionally graded porous plates with graphene platelets reinforcement. Thin-Walled Struct 150:106684
6. Shokrgozar A, Ghabussi A, Ebrahimi F, Habibi M, Safarpour H (2020) Viscoelastic dynamics and static responses of a graphene nanoplatelets-reinforced composite cylindrical microshell. Mech Based Des Struct Mach. https://doi.org/10.1080/15397734.2020.1719509
7. Tabatabaei-Nejhad S, Malekzadeh P, Eghtesad M (2020) Out-of-plane vibration of laminated FG-GPLRC curved beams with piezoelectric layers. Thin-Walled Struct 150:106678

8. Hosseini-Hashemi S, Ilkhani M, Fadaee M (2013) Accurate natural frequencies and critical speeds of a rotating functionally graded moderately thick cylindrical shell. Int J Mech Sci 76:9–20
9. Dong Y, Li Y, Chen D, Yang J (2018) Vibration characteristics of functionally graded graphene reinforced porous nanocomposite cylindrical shells with spinning motion. Compos B Eng 145:1–13
10. Dong Y, Zhu B, Wang Y, Li Y, Yang J (2018) Nonlinear free vibration of graded graphene reinforced cylindrical shells: effects of spinning motion and axial load. J Sound Vib 437:79–96
11. Qin Z, Safaei B, Pang X, Chu F (2019) Traveling wave analysis of rotating functionally graded graphene platelet reinforced nanocomposite cylindrical shells with general boundary conditions. Results Phys 15:102752
12. Dong Y, Zhu B, Wang Y, He L, Li Y, Yang J (2019) Analytical prediction of the impact response of graphene reinforced spinning cylindrical shells under axial and thermal loads. Appl Math Model 71:331–348
13. Qinkai H, Fulei C (2013) Parametric instability of a rotating truncated conical shell subjected to periodic axial loads. Mech Res Commun 53:63–74
14. Malekzadeh P, Heydarpour Y (2013) Free vibration analysis of rotating functionally graded truncated conical shells. Compos Struct 97:176–188
15. Heydarpour Y, Aghdam M, Malekzadeh P (2014) Free vibration analysis of rotating functionally graded carbon nanotube-reinforced composite truncated conical shells. Compos Struct 117:187–200
16. Shakouri M (2019) Free vibration analysis of functionally graded rotating conical shells in thermal environment. Compos B Eng 163:574–584
17. Banh TT, Shin S, Lee D (2018) Topology optimization for thin plate on elastic foundations by using multi-material. Steel Compos Struct 27:177–184
18. Nguyen AP, Banh TT, Lee D, Lee J, Kang J, Shin S (2018) Design of multiphase carbon fiber reinforcement of crack existing concrete structures using topology optimization. Steel Compos Struct 29:635–645
19. Banh TT, Lee D (2019) Topology optimization of multi-directional variable thickness thin plate with multiple materials. Struct Multidiscip Optim 59:1503–1520
20. Song M, Yang J, Kitipornchai S (2018) Bending and buckling analyses of functionally graded polymer composite plates reinforced with graphene nanoplatelets. Compos B Eng 134:106–113
21. Eltaher M, Alshorbagy A, Mahmoud F (2013) Determination of neutral axis position and its effect on natural frequencies of functionally graded macro/nanobeams. Compos Struct 99:193–201
22. Mirzaei M, Kiani Y (2015) Thermal buckling of temperature dependent FG-CNT reinforced composite conical shells. Aerosp Sci Technol 47:42–53
23. Affdl JH, Kardos J (1976) The Halpin–Tsai equations: a review. Polym Eng Sci 16:344–352
24. Reddy JN (2017) Energy principles and variational methods in applied mechanics. Wiley, New York
25. Li H, Lam K-Y, Ng T-Y (2005) Rotating shell dynamics. Elsevier, Amsterdam
26. Bert CW, Malik M (1996) Differential quadrature method in computational mechanics: a review. Appl Mech Rev 49:1–28
27. Genta G (2007) Dynamics of rotating systems. Springer, Berlin
28. Torabi K, Afshari H (2016) Exact solution for whirling analysis of axial-loaded Timoshenko rotor using basic functions. Eng Solid Mech 4:97–108
29. Torabi K, Afshari H, Najafi H (2017) Whirling analysis of axial-loaded multi-step Timoshenko rotor carrying concentrated masses. J Solid Mech 9(1):138–156
30. Afshari H, Irani Rahaghi M (2018) Whirling analysis of multi-span multi-stepped rotating shafts. J Braz Soc Mech Sci Eng 40:424
31. Afshari H, Torabi K, Jafarzadeh Jazi A (2020) Exact closed form solution for whirling analysis of Timoshenko rotors with multiple concentrated masses. Mech Based Des Struct Mach. https://doi.org/10.1080/15397734.2020.1737112
32. Dai Q, Cao Q, Chen Y (2018) Frequency analysis of rotating truncated conical shells using the Haar wavelet method. Appl Math Model 57:603–613
33. Liu F, Ming P, Li J (2007) Ab initio calculation of ideal strength and phonon instability of graphene under tension. Phys Rev B 76:064120
34. Rafiee MA, Rafiee J, Wang Z, Song H, Yu Z-Z, Koratkar N (2009) Enhanced mechanical properties of nanocomposites at low graphene content. ACS Nano 3:3884–3890
35. Yasmin A, Daniel IM (2004) Mechanical and thermal properties of graphite platelet/epoxy composites. Polymer 45:8211–8219
36. Liew KM, Ng TY, Zhao X (2005) Free vibration analysis of conical shells via the element-free kp-Ritz method. J Sound Vib 281:627–645
37. Shu C (1996) An efficient approach for free vibration analysis of conical shells. Int J Mech Sci 38:935–949